

CoSHA: Code for Stellar properties Heuristic Assignment – for the MaStar stellar library

ALFREDO MEJÍA-NARVÁEZ¹ AND GUSTAVO BRUZUAL²

SEBASTIAN. F. SÁNCHEZ¹

LETICIA CARIGI¹

JORGE BARRERA-BALLESTEROS¹

MABEL VALERDI¹

RENBIN YAN³

NIV DRORY⁴

¹*Instituto de Astronomía, Universidad Nacional Autónoma de México*

A. P. 70-264, C.P. 04510

México, D.F., México

²*Instituto de Radioastronomía y Astrofísica, Universidad Nacional Autónoma de México*

Campus Morelia, Michoacan

México C.P. 58089, México

³*Center for Astrophysical Sciences, Department of Physics and Astronomy,*

Johns Hopkins University,

Baltimore, MD 21218, USA

⁴*McDonald Observatory, Department of Astronomy,*

University of Texas at Austin, 1 University Station,

Austin, TX 78712-0259, USA

(Received January 1, 2018; Revised January 7, 2018; Accepted June 21, 2022)

Submitted to ApJ

ABSTRACT

We introduce CoSHA: a Code for Stellar properties Heuristic Assignment. In order to estimate the stellar properties, CoSHA implements a Gradient Tree Boosting algorithm to label each star across the parameter space (T_{eff} , $\log g$, $[\text{Fe}/\text{H}]$, and $[\alpha/\text{Fe}]$). We use CoSHA to estimate these stellar atmospheric parameters of 22k unique stars in the MaNGA Stellar Library (MaStar). To quantify the reliability of our approach, we run both internal tests using the Göttingen Stellar Library (GSL, a theoretical library) and the first data release of MaStar, and external tests by comparing the resulting distributions in the parameter space with the APOGEE estimates of the same properties. In summary, our parameter estimates span in the ranges: $T_{\text{eff}} = [2900, 12000]$ K, $\log g = [-0.5, 5.6]$, $[\text{Fe}/\text{H}] = [-3.74, 0.81]$, $[\alpha/\text{Fe}] = [-0.22, 1.17]$. We report internal (external) uncertainties of the properties of $\sigma_{T_{\text{eff}}} \sim 48$ (325) K, $\sigma_{\log g} \sim 0.2$ (0.4), $\sigma_{[\text{Fe}/\text{H}]} \sim 0.13$ (0.27), $\sigma_{[\alpha/\text{Fe}]} \sim 0.09$ (0.14). These uncertainties are comparable to those of other methods with similar objectives. Despite the fact that CoSHA is not aware of the spatial distribution of these physical properties in the Milky Way, we are able to recover the main trends known in the literature with great statistical confidence. The catalogue of physical properties can be accessed in <http://ifs.astroscu.unam.mx/MaStar>.

Keywords: stars — atmospheric parameters — statistics — machine learning

1. INTRODUCTION

The interpretation of galaxy observations into stellar physical properties ultimately relies on a set of ingredients, namely: a selection of stellar evolutionary tracks, an initial mass function and a stellar spectral library (e. g., Bruzual & Charlot 2003; Maraston 2005; Conroy et al. 2009). While, the first two are better constrained through our theoretical knowledge of the stellar interiors and stellar evolution, the latter provides the fundamental link between such theoretical knowledge and the observable quantities. In its essence, a stellar library is a collection of stellar spectra as homogeneous (in sampling and resolution) and curated (from instrumental and flux calibration artifacts) as possible, in the spectral space (e. g., Terndrup et al. 1990; Lancon & Rocca-Volmerange 1992; Fluks et al. 1994). In the parameter space, usually defined by T_{eff} , $\log g$, $[\text{Fe}/\text{H}]$, and $[\alpha/\text{Fe}]$, the distributions of stars in the library are expected to span the range of plausible physics according to the theory, also in an homogeneous way.

These requirements present several challenges since stellar surveys are mostly limited to our galaxy and, in some cases, further limited to the solar neighborhood (e. g., Le Borgne et al. 2003; Valdes et al. 2004; Sánchez-Blázquez et al. 2006; Chen et al. 2014). Such limitations in our ability to acquire large samples of stars, eventually lead to a poor sampling of parameter space. Furthermore, these limitations are exacerbated by the fact that most galaxies (including our own) usually display heterogeneous distributions in their stellar contents (e. g., Hayden et al. 2015; Fernández-Alvar et al. 2017; Helmi et al. 2018; Barbuy et al. 2021). Therefore it is of paramount importance to better sample our own galaxy and eventually other galaxies with a large spatial coverage and a high spectral resolution. To mitigate these restrictions in parameter space sampled in these so called *empirical* stellar libraries, several groups of authors have implemented *theoretical* stellar libraries (e. g., Lejeune et al. 1997; Lejeune et al. 1998). Conceptually, theoretical libraries should be able to overcome the issue of sampling in parameter space. However in practice, this flexibility comes at a cost: a poor sampling in spectral space. Therefore in order to implement a theoretical library, a trade-off has to be made in observed space, mainly due to incomplete theoretical knowledge about stellar atmosphere opacities and/or incomplete atomic and molecular data (see Conroy 2013, and references therein).

Both empirical and theoretical libraries are clearly complementary approaches (see Coelho et al. 2020). As a matter of fact, most commonly used synthesis of stellar population models combine both, in order to improve the accuracy in their predictions (e. g., Cid Fernandes et al. 2014). In this sense, the MaNGA Stellar Library (MaStar Yan et al. 2019) comprising (at present) 24.4k stars in the same footprint of the MaNGA survey, promises to be a huge leap forward in the direction of a better sampling of parameter space while preserving the completeness of spectral features in the optical range of empirical libraries.

A major challenge is to calibrate such data set in T_{eff} , $\log g$, $[\text{Fe}/\text{H}]$ and $[\alpha/\text{Fe}]$. In this work we introduce a new method to determine atmospheric physical parameters of the MaStar spectra by implementing a machine learning (ML) algorithm called Gradient Tree Boosting (GTB). GTB is an ensemble method that successively trains a predefined number of decision trees, each improving upon its predecessor errors. This paper is organized as follows. In § 2 we describe the MaStar data set and the data sets used for training and testing, the quality controls taken and the pre-processing for homogenizing the spectra; in § 3 we present the physical parameter estimator and training process; in § 4 we evaluate the physical parameters using a set of internal and external tests, and in § 5 we present the MaStar stellar library physical properties; finally, we conclude in § 6.

2. DATA AND SAMPLES

2.1. Observations

MaNGA is an integral field spectroscopy survey of 10,000 nearby galaxies (Bundy et al. 2015; Law et al. 2015; Yan et al. 2016; Wake et al. 2017) as part of the SDSS-IV along with other two surveys: eBOSS (Dawson et al. 2016) and APOGEE-2 (Majewski et al. 2017). It uses the Baryon Oscillation Spectroscopic Survey spectrographs (Smee et al. 2013), fiber-fed using different fiber bundle configurations for science targets, standard stars and sky observations (Drory et al. 2015). The wavelength sampling of the spectrographs combined covers $\sim 2600 - 10000 \text{ \AA}$ with an average resolution of $R = 1800$. In order to make observations of different fields during one night, the fiber-plugged plates are stored in housings called cartridges. MaNGA shares six out of nine cartridges with APOGEE-2. This configuration presented the opportunity to piggyback on the APOGEE survey to build the MaStar stellar library.

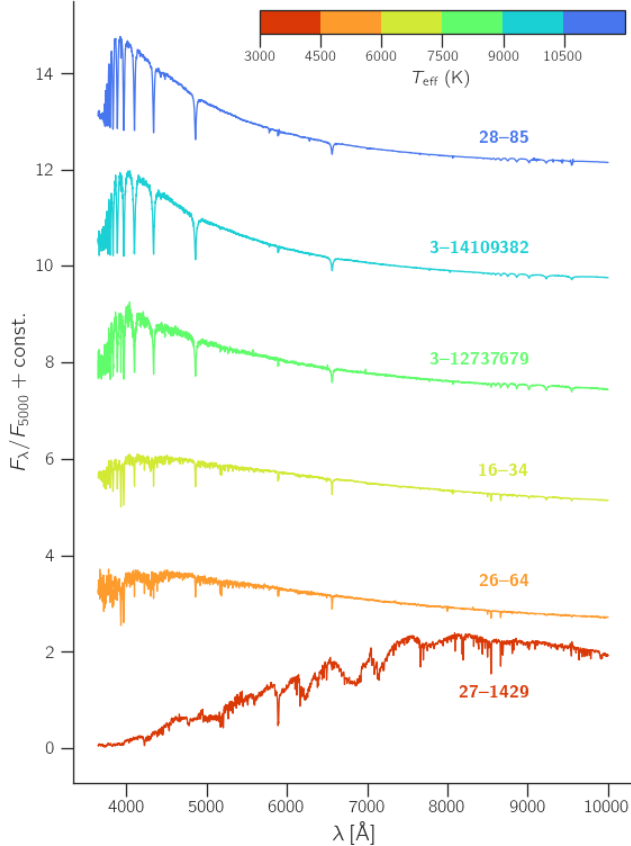


Figure 1. Examples of the spectra in the MaStar library color coded according to their T_{eff} . The first data release of the library spans a wide range of the physical parameter space suitable for training a machine learning (ML) model to predict the properties of the rest of the stellar spectra.

The observing strategy, target selection and data reduction are detailed in Yan et al. (2019).

2.2. Samples

Since we intend to use a ML method, we have to be aware that one of the most important challenges when it comes to this approach is the need for a clean, complete and already labelled sample. In this particular case, in order to predict reliable estimates of T_{eff} , $\log g$, $[\text{Fe}/\text{H}]$ and $[\alpha/\text{Fe}]$ for the MaStar spectra, we need a sample of stellar spectra with reliable estimates of these same properties. In the previous section we already sketch out the difficulties of having such empirical library at our disposal. However, state-of-the-art theoretical libraries do prove to be a suitable option.

In the literature there are plenty of theoretical libraries, most of which are focused on particular types of stars (e. g., Kirby 2011; Coelho 2014). However, we require a multi-purpose theoretical stellar library in order to build models as general as possible. For this pur-

pose we choose the Göttingen Spectral Library (GSL; Husser et al. 2013, ~ 27 k stars). The GSL is a stellar spectral library based on the latest version of the stellar atmospheric parameter code PHOENIX (Hauschildt et al. 1999). This library offers the following advantages for our study: (i) it samples a wide range of stellar stages, from sub-dwarf up to super giant stars ($\log g = 0.0 - 6.0$), and spectral types ($T_{\text{eff}} = 2300 - 12000$ K); (ii) it predicts non-solar abundance patterns ($[\text{Fe}/\text{H}] = -4.0 - +1.0$ and $[\alpha/\text{Fe}] = -0.2 - +1.2$) in a mostly homogeneous fashion; (iii) it implements the latest atomic and molecular data, and opacity solutions to predict high-resolution spectra ($R \sim 500$ k in $\lambda = 3000 - 25000$ Å). We acknowledge that perhaps two important weaknesses of the GSL is the lack of stars hotter than 12000 K and α -enhanced/depleted atmospheres for stars outside the ranges $-3 \leq [\text{Fe}/\text{H}] \leq 0$ and $3500 \leq T_{\text{eff}} \leq 8000$ K. For more details on the GSL, we refer the reader to Husser et al. (2013) and references therein.

In an attempt to mitigate some of the above-mentioned deficiencies of the GSL, we also adopt the physical properties included in the first data release of MaStar (Yan et al. 2019, ~ 3 k stars). The MaStar stellar properties presented in Yan et al. (2019, hereafter MaStarDR1) are a compilation of the properties reported by the APOGEE (Majewski et al. 2017), SEGUE (Yanny et al. 2009) and LAMOST (Cui et al. 2012) surveys, all of which are based on different kind of observations and analysis methods (García Pérez et al. 2016; Lee et al. 2008; Xiang et al. 2015, respectively). These methods mostly implement algorithms based on template matching of spectroscopic and or photometric data to other (well-determined) observed or theoretical stellar libraries or a combination thereof. In particular, Lee et al. (2008) also implements an Artificial Neural Network algorithm in part of their analysis to estimate atmospheric stellar properties. We stress that the atmospheric parameters reported in Yan et al. (2019) are intended to aid the target selection of the MaStar stellar library and not to be used on stellar population analysis. Furthermore, the fact that most of these stellar properties are derived from different wavelength ranges, signal-to-noise levels and using different types of analysis methods, we may expect different sources of uncertainties (not present in a theoretical library such as GSL) to propagate during the training stage.

2.3. Quality control

Before we can analyse the MaStar spectra, we need to ensure the quality of the observations. In this section we present the quality control steps employed in this work.

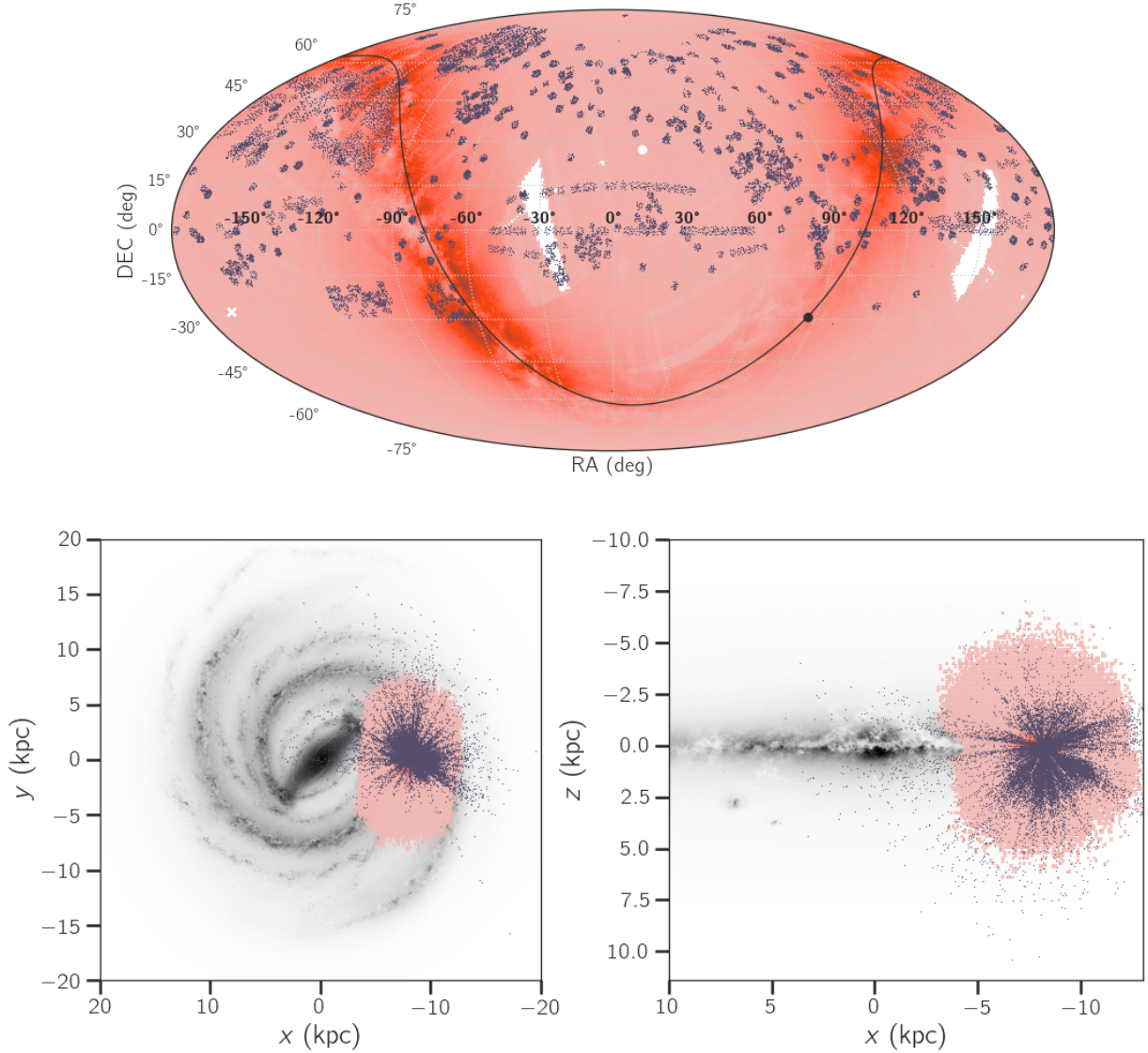


Figure 2. The spatial distribution of the MaStar stars in the cleaned sample (purple) compared to that of the Gaia DR2 (orange). *top:* the distribution in right ascension (RA) and declination (DEC) shows the in-homogeneous sampling of the MaStar. *bottom:* the distribution of MaStar in the galactic projections $x - y$ (left) and $x - z$ (right) demonstrates that MaStar extends well beyond the solar neighborhood. Lower panel plots were generated using the Python package <https://pypi.org/project/mw-plot/0.3.0/>.

In this section we explain the measures we take in order to have the best possible spectra to train the model.

In the MaStar library, the stars have been observed under different atmospheric conditions, using different total integration times and most of them have been observed in several visits (~ 3 per star on average). In total there are $\sim 68.2\text{k}$ visits. It is expected that some visits to the same star may have better quality than others. In order to ensure that we keep only the best quality data, we use a series of internal quality flags and estimated parameters provided by **MaStarDR1**, namely:

MJDQUAL: describes the quality of the spectroscopic calibration.

MNGTARG2: describes the quality of the photometric selection.

RADVEL: the radial velocity. Stars with no measure of this parameter are flagged as bad.

The first two are bit mask flags. **MJDQUAL** is required not to have bits 1, and 4, \dots , 9. i. e., each spectrum is required to have: good sky subtraction, good point spread function (PSF) fitting, good estimates of the extinction, good estimation of the radial velocity (scatter lower than 10 km s^{-1} across multiple exposures), good calibration after visual inspection, no emission line in $\text{H}\alpha$ with equivalent width greater than 0.6\AA , good signal-to-noise per pixel (median > 50). **MNGTARG2** is required not to

have bit 15 activated, this means that the photometric selection is reliable.

After selecting the best quality data according to the aforementioned flags, our sample comprises 24.4k good quality spectra of unique stars ($\sim 98.5\%$ of the original sample). In Fig. 1 we show several examples of the spectra in the MaStar library color-coded according to their T_{eff} as reported in MaStarDR1.

Even though we effectively keep the best quality spectra from the internal flags described above, some spectra may still remain with notable artifacts due to imperfect flagging in the first place. There are several common issues: emission lines, noisy spectra, bad continuum calibration and missing pixels.

In order to further mitigate bad continuum calibration we use the Gaia DR2 (Brown et al. 2018). We select only those stars from the MaStar library that have been catalogued by Gaia and that have a reliable astrometry and photometry (Evans et al. 2018). In addition, we derive the synthetic magnitude in the Gaia photometric system (G_{bp} , G_{rp} and G) from the spectra of the MaStar matched library. Then we select those stars with: (i) realistic blue Gaia color ($G_{\text{bp}} - G_{\text{rp}} \geq -0.76$ mag), due to flux calibration issues; (ii) a parallax > 0.05 mas; and (iii) a median signal-to-noise ratio $S/N \geq 20$ along the entire wavelength range. After cleaning the sample, we keep ~ 22 k stars with reliable flux calibration and S/N .

In Fig. 2 we show the spatial distribution of the MaStar stars in the cleaned sample, compared to that of Gaia. The in-homogeneous sampling of MaStar given the multi-fiber nature of the survey. None the less, it is clear that MaStar samples different regions of the Milky Way and is not limited to the solar neighborhood, within the declination limits of the survey.

2.4. Pre-processing

In this section we implement ML algorithms. The unfamiliar reader may refer to § A to briefly get acquainted on the common ML jargon and the notation adopted throughout this study. We encourage the seasoned reader to skip § A altogether.

To solve the problems related to the presence of emission lines and the missing pixels, we implement two separate unsupervised ML algorithms: an outlier detection method and a missing features (pixels) filler. Both of these algorithms are based on the k -nearest neighbors algorithm (KNN, Fix & Hodges 1951). In a nutshell, the KNN algorithm consists on finding the closer k samples (e. g., in an Euclidean sense) to each sample spectrum. In the following we elaborate on the usage of the KNN to remove emission lines and to fill-in missing pixels.

For the emission line problem, we implement the Local Outlier Factor (LOF) algorithm (Breunig et al. 2000), from the SCIKIT-LEARN Python library (Pedregosa et al. 2011a). The problem is posed as follows: given an observed spectrum $f_{\text{obs}} = (\lambda_i, f_i)$ for $i = 1, \dots, n$, this method looks for under-densities in the locality of each pixel (λ_i, f_i) . Such locality is defined by the k -nearest neighbors to (λ_i, f_i) and the surrounding density is measured using the distance between those neighbors. In this case we define an Euclidean distance between each pair (λ_i, f_i) and the rest of the spectrum pixels. A pixel is then flagged as outlier (and turned into missing a pixel) if its local density is smaller than a factor of the density of its k -neighbors. Given the nature of the stellar spectral energy distributions, this algorithm is prone to produce a large fraction of false positives (e. g., absorption lines). In order to regularize the LOF algorithm, we set $k = 5$ and the expected contamination for emission lines to be 0.4%. This way we improve the accuracy of the emission line detection.

For the missing pixel problem, we implement the KNN “imputer” (filler) algorithm (Troyanskaya et al. 2001). Essentially, given a spectrum observed in the wavelength range $f_{\text{obs}} = (\lambda_i, f_i)$ for $i = 1, \dots, n$ with missing values in an arbitrary sub-subset of wavelengths $\lambda_{\text{missing}} \in \{\lambda_m\} \subset \lambda_{\text{obs}}$, this method looks for the KNN spectra in the library with no missing values in λ_{missing} and then computes a distance-weighted average spectrum defined in λ_{missing} to fill-in the missing values.

2.5. Volume correction

The MaStar library is intended to provide a homogeneous and complete coverage of the parameter space in T_{eff} , $\log g$, $[\text{Fe}/\text{H}]$, and $[\alpha/\text{Fe}]$. Hence, by construction, the corresponding physical properties are not representative of all the stellar populations in the Milky Way, i. e. intrinsically rare stars may be over-represented. In order to reliably compare the distributions of these physical properties with those already known from other (volume-complete) surveys, we first need to make a volume correction. In principle, we would need a sample of the stars representative of all the Milky Way stellar populations. However, to the best of our knowledge such data set does not exist. Our best choice to date is to use the Gaia survey DR2 (Brown et al. 2018), containing well over 60 M unique stars and complete down to 12 mag in the G band. Since the Gaia survey is not volume-complete and the MaStar sample is not representative of all plausible stars, this is a *partial* volume correction (Bailer-Jones et al. 2018). Therefore, the volume corrected MaStar sample is only representative of the stellar populations (as seen in the color-magnitude

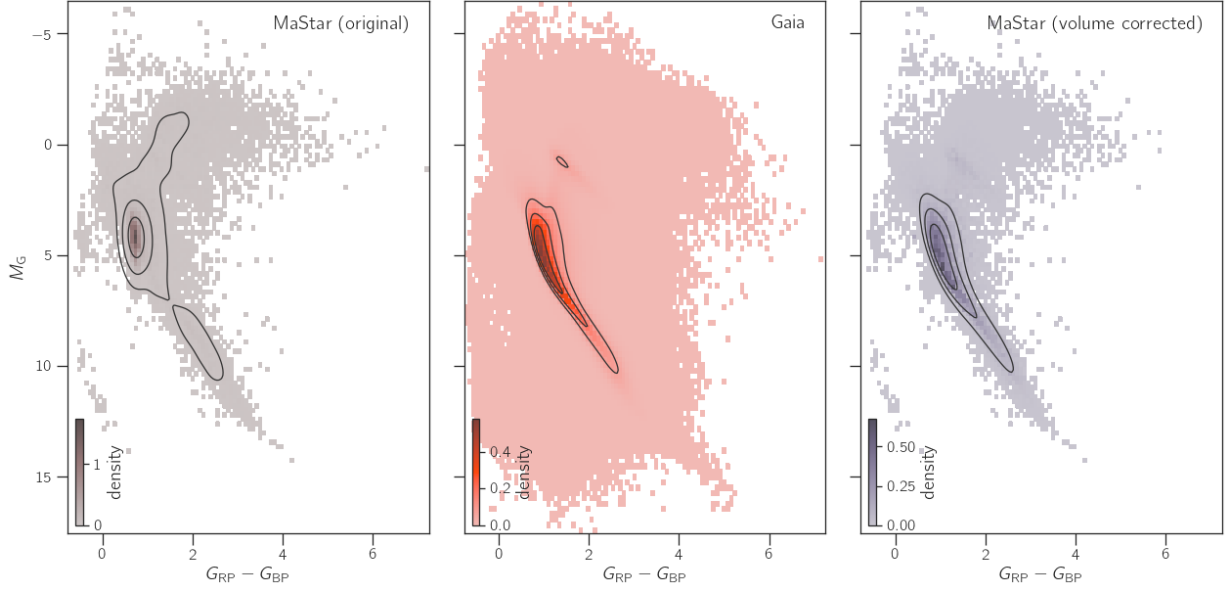


Figure 3. CMD of the MaStar library (left), Gaia DR2 (middle) and the volume corrected version of MaStar (right) are shown. The similarity in the shape of the middle and right distributions shows that the volume correction is accurate.

distribution) sampled by the Gaia survey (Evans et al. 2018; Arenou et al. 2018).

We compute the volume correction using the distribution of stars in the color-magnitude diagram (CMD). Mathematically, we express the volume as:

$$V \equiv \frac{\text{PDF}_{\text{MaStar}}}{\text{PDF}_{\text{Gaia}}}, \quad (1)$$

where the $\text{PDF}_{\text{MaStar}}$ and PDF_{Gaia} are the corresponding probability density distributions of observing stars in the CMD for the corresponding catalogue. In Fig. 3 we show the original distribution in the MaStar (left), the Gaia distribution (middle) and the corrected MaStar distribution (right).

2.6. Training and testing sets

Once we have cleaned the sample and pre-processed the spectra, we select the training and the testing subsets. We arrange the spectra (MaStarDR1+GSL) into a $N_{\text{spec}} \times N_{\text{pix}}$ matrix, so that each row is a spectrum and each column is a wavelength pixel. We will refer to this matrix as the *features matrix*, denoted by \mathbf{X} . Correspondingly, each spectrum in the features matrix will be characterized by the set of parameters (T_{eff} , $\log g$, $[\text{Fe}/\text{H}]$, $[\alpha/\text{Fe}]$), arranged into a $N_{\text{spec}} \times 4$ *labels matrix*, \mathbf{Y} . It is the goal of this study to train a model using the features matrix to translate new observations (records in the features matrix) into its corresponding physical properties.

It is important that the training and the testing subsets are not biased against common types of stars (e. g., dwarfs). This is to ensure that the trained model is as

general as possible and can predict stellar properties of any kind of stars. From the stellar spectra libraries discussed in the § 2, only GSL fulfills these requirements, albeit with the intrinsic limitations of a synthetic stellar library. Therefore, we select a random subset comprising 90% of the stars in the GSL to be part of the training set. In order to avoid hampering the estimator during training with stellar spectral lacking the common instrumental and calibration artifacts (e. g., low S/N , emission lines, sky subtraction and flux calibration), we also include as part of the training a random subset of 90% of the MaStar DR1 spectra. The training subset comprises ~ 27 k stars out of the total of ~ 30 k stellar spectra with good estimation of the physical parameters. The remaining 10% (~ 3 k) of the GSL+MaStarDR1 stars are devoted to test the parameter estimator after training. Since most of the stars in these subsets have well known physical properties, the testing selection is suitable for the set proposes. In Fig. 4 we show the distribution of the parameters in the GSL+MaStarDR1 sample (grey), and the corresponding segregation by stellar library (GSL: blue, MaStarDR1: red) and by subset (training: solid line, testing: dashed line), both represented by 99% confidence contours. As expected the GSL stellar library follows a nearly uniform distribution across the parameter space, while the MaStarDR1 draws a distribution that resembles the observed trends in stellar populations (e. g. in the solar neighborhood). The fact that the training and testing subsets have similar distributions, regardless of the stel-

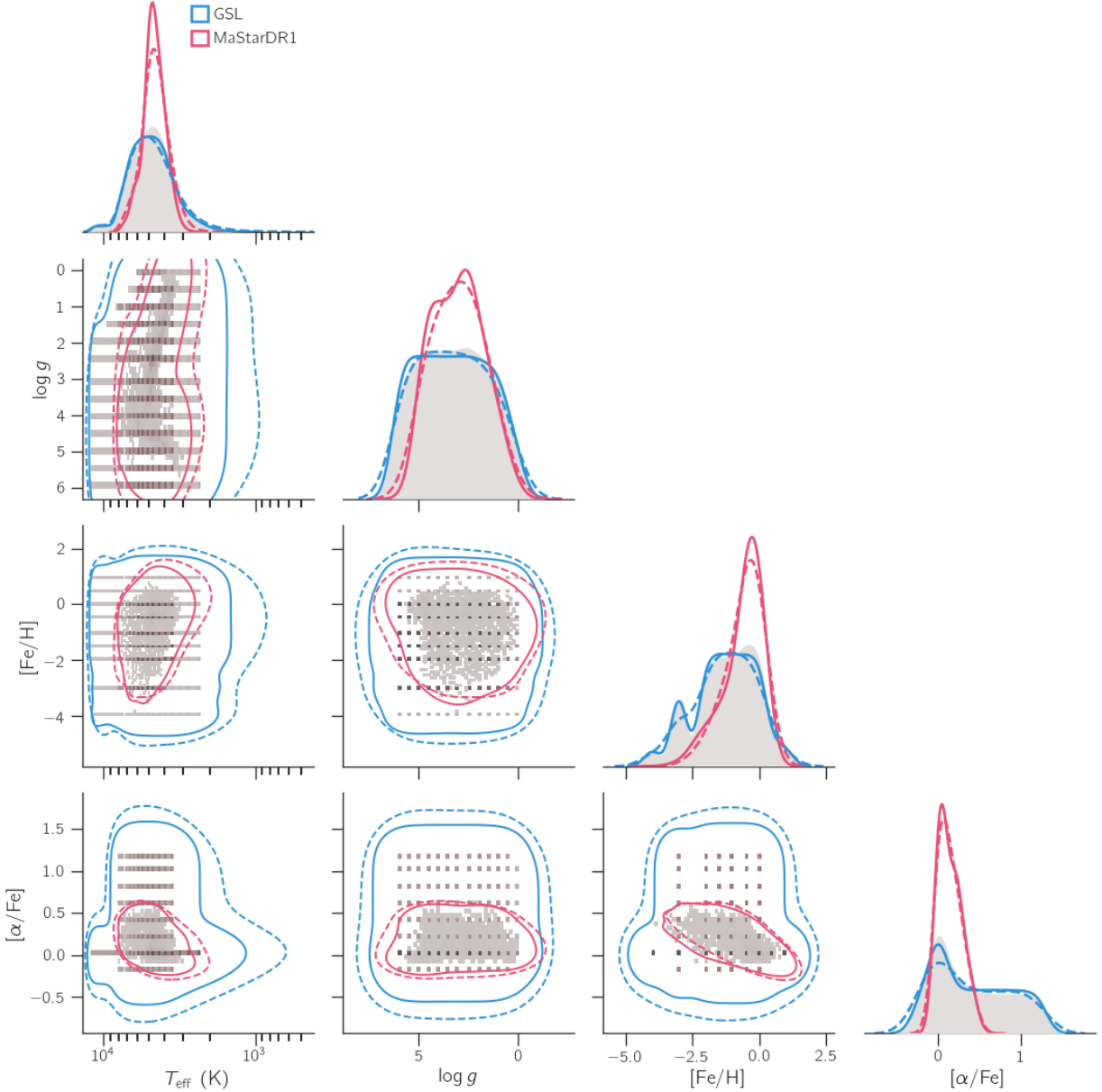


Figure 4. We show the distribution of physical parameters (T_{eff} , $\log g$, $[\text{Fe}/\text{H}]$ and $[\alpha/\text{Fe}]$) in a set of paired diagrams and histograms for the full sample of 30 k star spectra with a good determination of the stellar properties (GSL+MaStar DR1, grey values), together with the 99% confidence region (contours) of the adopted training (solid) and testing (dashed) subsets corresponding to the GSL (blue) and MaStarDR1 (red) libraries. Clearly GSL spans a wider range of stellar properties than the MaStar DR1. See text in § 2.6 for details.

lar library, is indicative that the testing procedure will be robust, despite the much smaller size of this subset.

In the next section we elaborate on the algorithm adopted for the parameter estimator, the training and the testing procedures. We will refer to the corresponding subsets as $\mathbf{X}_{\text{train}}$, $\mathbf{Y}_{\text{train}}$ and \mathbf{X}_{test} , \mathbf{Y}_{test} , respectively.

3. THE PROPERTIES ESTIMATOR: CoSHA

Most ML algorithms can be mathematically expressed as a functional $\mathcal{F}(\boldsymbol{\theta}, \boldsymbol{\phi})$ where $\boldsymbol{\theta}$ is a vector of parameters that define the trained (fitted) model and $\boldsymbol{\phi}$ is the vector of hyper-parameters that define how the model will be trained (e. g., the merit or loss function, optimization algorithm, etc.). Once the hyper-parameters are set, $F \equiv \mathcal{F}(\boldsymbol{\theta}, \boldsymbol{\phi})$, the algorithm is ready to train a model $\hat{F} = F(\mathbf{X}_{\text{train}}, \mathbf{Y}_{\text{train}})$. The training process to build \hat{F} , consists in maximizing (minimizing) the score (loss) function in order to find the optimal set of param-

eters, $\hat{\theta}$. Once trained, the fitted model should be able to provide reliable predictions given a set of features from new observations (not seen during the training). In reality, most problems require further exploration of the hyper-parameter space during the training phase in order to ensure robust results. However, in order to save computational time, we adopt an heuristic approach to train an *ad-hoc* selection of hyper-parameters.

In this study we implement a Gradient Tree Boosting (GTB) algorithm to train a model suitable for predicting the physical properties of the MaStar spectra. The GTB has two interesting characteristics, namely: it is an ensemble method and it is based on decision trees. Given the relatively small training set (27.4k spectra), a decision tree based method is a convenient option, as opposed to a more sophisticated approach such as training an artificial neural network. The latter would require, in general, hundreds of thousands of spectra (depending on the actual number of features), in order to yield reliable results. Another important advantage of the SCIKIT-LEARN of GTB implementation is that it allows for quantile regression, a type of regression in which it is possible to estimate any quantile of the probability distribution of \mathbf{Y} conditional on \mathbf{X} , $P(\mathbf{Y}|\mathbf{X})$. Hence, this type of regression is more general as it is not limited to finding the mean of that distribution, \hat{F} . In order to train a quantile regression estimator, we change the hyper-parameters of the GTB algorithm accordingly and set to predict the 16th and 84th percentiles (P_{16} and P_{84} , respectively).

The fact that GTB is an ensemble algorithm means that it is the combination of several individual estimators (in this instance, decision trees). The boosting character of this algorithm comes from the fact that each trained decision tree improves its predecessor. This last trait of the GTB algorithm entails more robust results than single-estimator algorithms. A GTB is therefore a type of ensemble composed by a predefined number of n decision trees, that can be expressed as the summation:

$$\hat{F} = f_0(\mathbf{X}_{\text{train}}, \mathbf{Y}_{\text{train}}) + \sum_{i=1}^{n-1} f_i(\mathbf{X}_{\text{train}}, \Delta \mathbf{Y}_i), \quad (2)$$

where f_0 is the first decision tree trained on the original training subset ($\mathbf{X}_{\text{train}}$ and $\mathbf{Y}_{\text{train}}$) and the successive f_i ($i > 0$) are the decision trees trained on the original training spectra ($\mathbf{X}_{\text{train}}$) but using as labels the residual between the original labels and the label predicted by the previous estimator, $\Delta \mathbf{Y}_i \equiv \mathbf{Y}_{\text{train}} - \hat{f}_{i-1}(\mathbf{X}_{\text{train}})$.

We acknowledge GTB carry some caveats, such as the loss of the easiness of the interpretation of its results, since it is built upon the combination of several trained

models. Furthermore, the actual training of the GTB must be done in a serial fashion, hence, it is computationally expensive to run an exhaustive search of the hyper-parameter space.

Finally, we use the trained model in \hat{F} to predict the stellar properties from the entire clean spectral library, to build the matrix $\mathbf{Y}_{\text{model}}$. We also use the estimators trained for the percentiles P_{16} and P_{84} to predict the precision of CoSHA by computing $\sigma_{\mathbf{Y}} = (P_{84} - P_{16})/2$, which under the assumption of a $P(\mathbf{Y}|\mathbf{X})$ Gaussian distribution is equivalent to the standard deviation. In the following sections we evaluate the internal reliability of the resulting distributions in $\mathbf{Y}_{\text{model}}$ in the stellar parameter space.

4. MODEL EVALUATION

In this section we evaluate the reliability of the method described in the previous sections. We run two types of tests: internal and external. In the internal tests we look for the model accuracy on the testing set. We also look for trends between the residuals of our method and the true values in this subset.

Quantitatively, we measure the accuracy of the model through the residual defined as:

$$\Delta \mathbf{Y} \equiv \mathbf{Y}_{\text{model}} - \mathbf{Y}_{\text{true}}, \quad (3)$$

where $\mathbf{Y}_{\text{model}} \equiv \hat{F}(\mathbf{X})$, \mathbf{X} is any set of spectral features for which we know the corresponding set of true properties, \mathbf{Y}_{true} . We adopt the mean and the standard deviation of these residuals as an estimation of the systematic and random errors, respectively.

In the external tests, on the other hand, we compare the predictions of CoSHA with the values published in external catalogues, namely: the MaStar DR1 (MaStarDR1) and APOGEE DR15 (Majewski et al. 2017; Holtzman et al. 2018). We restricted this comparison to those stars covered by both samples. This comparison only accounts for the consistency between the methods being compared, and not the absolute accuracy of the procedure. We estimate the level of consistency (δ_{other}) through the definition of the discrepancy (not to be confused with the residual above) between the two predictions, as:

$$\delta_{\text{other}} \mathbf{Y} \equiv \mathbf{Y}_{\text{model}} - \mathbf{Y}_{\text{other}}, \quad (4)$$

where $\mathbf{Y}_{\text{other}}$ is the estimation performed by other authors on the same sample of stars.

Since the MaStarDR1 data set is part of the training/testing subsets, we reckon this is not an independent nor fair comparison. Nonetheless, the consistency between CoSHA predictions and those of MaStarDR1 is still interesting and deserves some exploration.

4.1. Precision

We quantify CoSHA precision using the quantile predictions as outlined in the previous section. In Fig. 5 we show the map of CoSHA precision in the $\log g$ versus T_{eff} plane. The contours represent the density distribution of stars. Clearly the loci of more precise determinations are not consistent with the locus of the highest star density. This seems to indicate that the origin of such (im)precision is not due to number statistics. The fact that most imprecise predictions correspond to temperature boundaries indicates that stars at the extrema of the parameter space are likely to have unreliable determinations. Unfortunately given the method implemented in CoSHA, the determination depends on the existence of a comprehensive set of spectra (either theoretical or observed) with good quality stellar properties spanning an as wide as possible parameter space.

4.2. Accuracy

In this section we use the testing subset of stars to measure the internal reliability (accuracy and precision) of CoSHA. Since a large percentage ($\sim 90\%$) of this testing subset corresponds to stars in the GSL, for these stars we can safely assume that we know the true values of the atmospheric properties studied in this work. Hence, we use the GSL stars to quantify the *internal* accuracy and precision of our method. The rest of the testing subset corresponds to MaStarDR1's estimates and will be used to quantify the consistency between both methods. In Fig. 6 we show the residuals (c. f. Eq. 3) in the parameter space. The grey distributions represent the testing subset, while the GSL and MaStarDR1 subsets are represented (as in Fig. 4) in blue and red, respectively. The contours enclose 1σ of the corresponding probability distributions. We reckon that this kind of plot can reveal potential dependencies amongst the physical properties, or the lack thereof. These correlations are commonly known as degeneracies.

In general, all projections in the entire residual space (grey distributions) shows almost no correlations. The accuracy is $\sim -2\text{K}$ in T_{eff} and $\sim 0.01\text{dex}$ (at most) for the rest of the properties. However the segregation of the testing subset into GSL (solid blue) and MaStarDR1 (solid red) subsets uncovers that their individual accuracies are rather different. The comparison between these distributions (blue and red) shows that our method is both more accurate and precise than MaStarDR1, across the parameter space. We recall though, that GSL residuals represent the real (internal) errors of our method while the residuals in the MaStarDR1 subset combines both CoSHA and MaStarDR1 errors. Albeit, we can estimate the MaStarDR1 intrinsic residuals

as a Gaussian distribution with $\mu = \mu_{\text{Y19}} - \mu_{\text{GSL}}$ and $\sigma = \sqrt{\sigma_{\text{Y19}}^2 - \sigma_{\text{GSL}}^2}$ (dashed red). Since the Gaussian supposition has the potential to visually hint asymmetries and other non-Gaussian behaviors, we also show for the sake of completeness the corresponding Gaussian distribution for the GSL subset (dashed blue), using $\mu = \mu_{\text{GSL}}$ and $\sigma = \sigma_{\text{Y19}}$. The residuals with the GSL shows the accuracy and precision across the parameter space characterized by $\Delta T_{\text{eff}} \sim -3 \pm 48\text{K}$, $\Delta \log g \sim 0.00 \pm 0.20$, $\Delta [\text{Fe}/\text{H}] \sim 0.00 \pm 0.13$ and $\Delta [\alpha/\text{Fe}] \sim 0.00 \pm 0.09$. On the other hand for MaStarDR1, the *intrinsic* systematic and random errors notably larger: $\Delta T_{\text{eff}} \sim 6 \pm 241\text{K}$, $\Delta \log g \sim 0.06 \pm 0.47$, $\Delta [\text{Fe}/\text{H}] \sim -0.01 \pm 0.27$ and $\Delta [\alpha/\text{Fe}] \sim 0.01 \pm 0.12$.

4.3. Consistency with MaStarDR1

Fig. 7 shows the discrepancy in T_{eff} , $\log g$, $[\text{Fe}/\text{H}]$ and $[\alpha/\text{Fe}]$, as defined in Eq. 4, between the values estimated in this study and those reported in MaStarDR1. We only compare those stars for which MaStarDR1 made estimations in our clean sample ($\sim 2.8\text{k}$ stars). It is clear from these comparisons that T_{eff} is the most robust property (i. e. less independent on the methodology), having the best consistency ($< 10\%$ discrepancy) across the whole range. Both the mean and the standard deviation in the marginal distributions are in agreement within $\sim 2\text{K}$ and $\sim 22\text{K}$ for T_{eff} , and ~ 0.03 and $\sim 0.09\text{dex}$ for the rest of the properties, respectively. Since most of these stars belong to the training set ($\sim 90\%$), we expect an overall high consistency in this particular comparison. However, it is interesting to note that some trends may appear given the different methodologies adopted by MaStarDR1 and in this study. We note that these discrepancies are comparable to the MaStarDR1 intrinsic errors estimated in the previous section. This indicates that even though we used the MaStarDR1 spectra to train CoSHA, we are able to disentangle the typical (intrinsic) error of both methods above. Furthermore, the observed discrepancies in Fig. 7 are likely to be dominated by MaStarDR1 errors.

T_{eff} and $\log g$ discrepancies show almost no deviation from the Gaussian distribution. However, $[\text{Fe}/\text{H}]$ and $[\alpha/\text{Fe}]$ display clear trends with respect to the MaStarDR1 estimates. In the particular case of the $[\alpha/\text{Fe}]$, the distribution of discrepancies displays a negative slope with respect to the values reported by MaStarDR1: the higher the $[\alpha/\text{Fe}]$, the more inconsistent becomes our estimate with respect to MaStarDR1 estimate, in the negative sense. This inconsistency may originate in either method or (most likely) in both. Therefore we will need to compare to external estimates of these parameters in order to find clues on the origin of this trend.

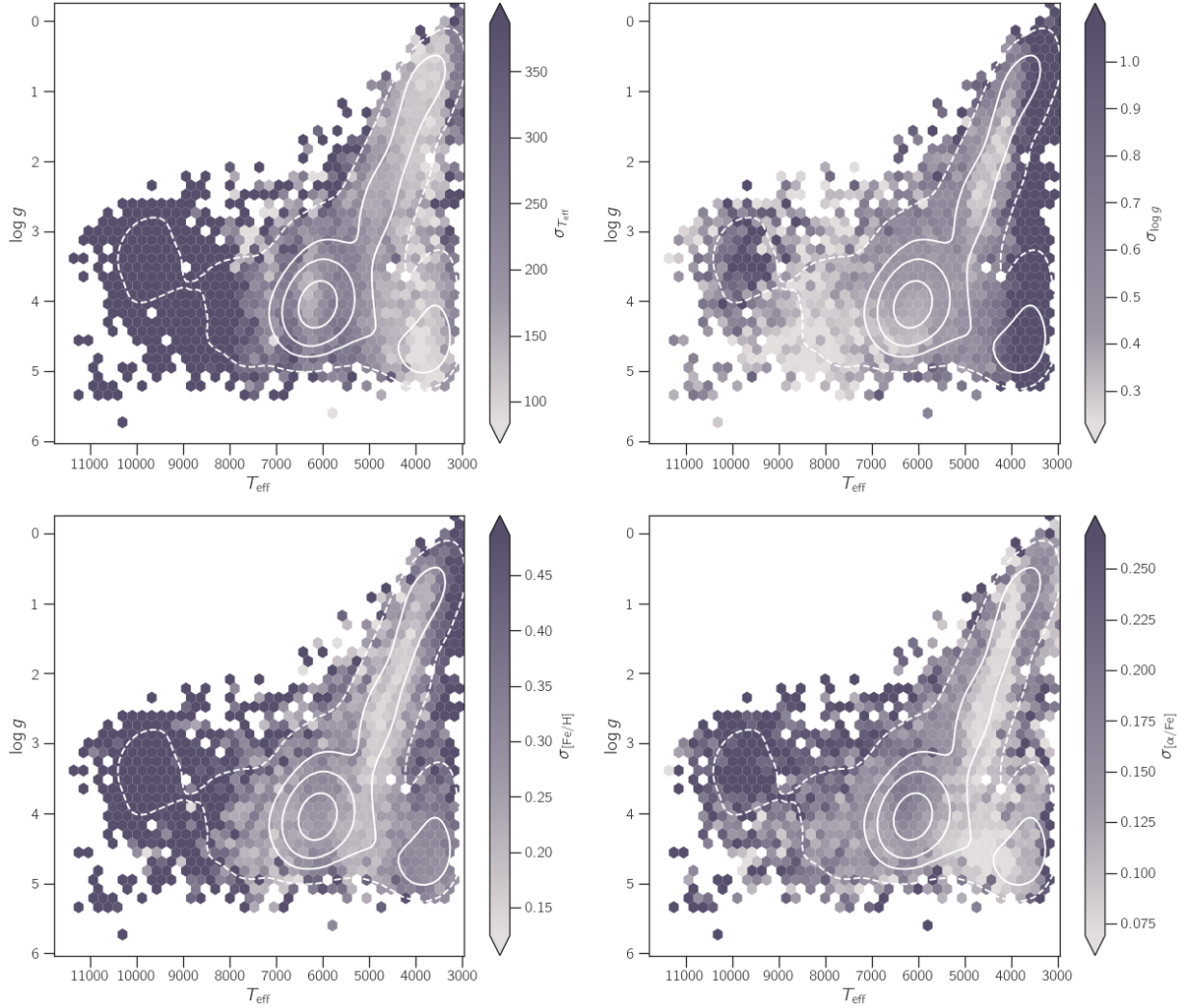


Figure 5. Distribution of the internal precision of COSHA in each predicted property in the $\log g$ vs. T_{eff} plane. The contours represent the density distribution at the quartiles (solid) and percentile 95th (dashed). The map of T_{eff} precision (upper left) shows increasingly large imprecision towards higher temperatures. The $\log g$ map reveals more imprecise results for the coolest stars. Both $[\text{Fe}/\text{H}]$ and $[\alpha/\text{Fe}]$ maps show increasing imprecision towards hotter and cooler stars. See text in § 4.1 for details.

4.4. Consistency with APOGEE

The APOGEE survey offers a great validation tool since it is known to have accurate distributions of T_{eff} , $\log g$ and abundances of several chemical species, including α -elements and Fe (e. g., [Hasselquist et al. 2020](#); [Nandakumar et al. 2020](#)). The APOGEE DR15 reports T_{eff} , $\log g$, $[\text{Fe}/\text{H}]$ and $[\alpha/\text{Fe}]$ values for most of the stars in the survey using two different methods: ASPCAP ([García Pérez et al. 2016](#)) and the CANNON ([Ness et al. 2015](#)). In the following we compare only with the original method developed for the APOGEE: ASPCAP, but see the Appendix B.1. Since the target selection for the MaStar survey results from the combination of piggy-backing on the APOGEE plates and cherry-picking to improve the sampling of the parameter space (specially in the T_{eff}), some stars in our clean sample of MaStar be-

long to the APOGEE survey, by construction. However, the sample cleaning described in § 2 and the match with Gaia to retrieve distances, cut the matching subset between MaStar and APOGEE down to just ~ 400 stars. In Fig. 8 we show the comparison between the physical properties derived by COSHA and those published by APOGEE for those stars in common in both surveys. As in the previous sections, we find that the T_{eff} determinations are the most consistent results, with most of the stars within the boundary of a 10% discrepancy (c. f. T_{eff} inset plot). Overall, we report a discrepancy with APOGEE in T_{eff} , in the mean and the standard deviation of the marginal distributions of ~ -45 and ~ 101 K, respectively. The distribution of $\log g$ show the larger scatter around the perfect consistency line. However the overall shape of the marginal distributions are

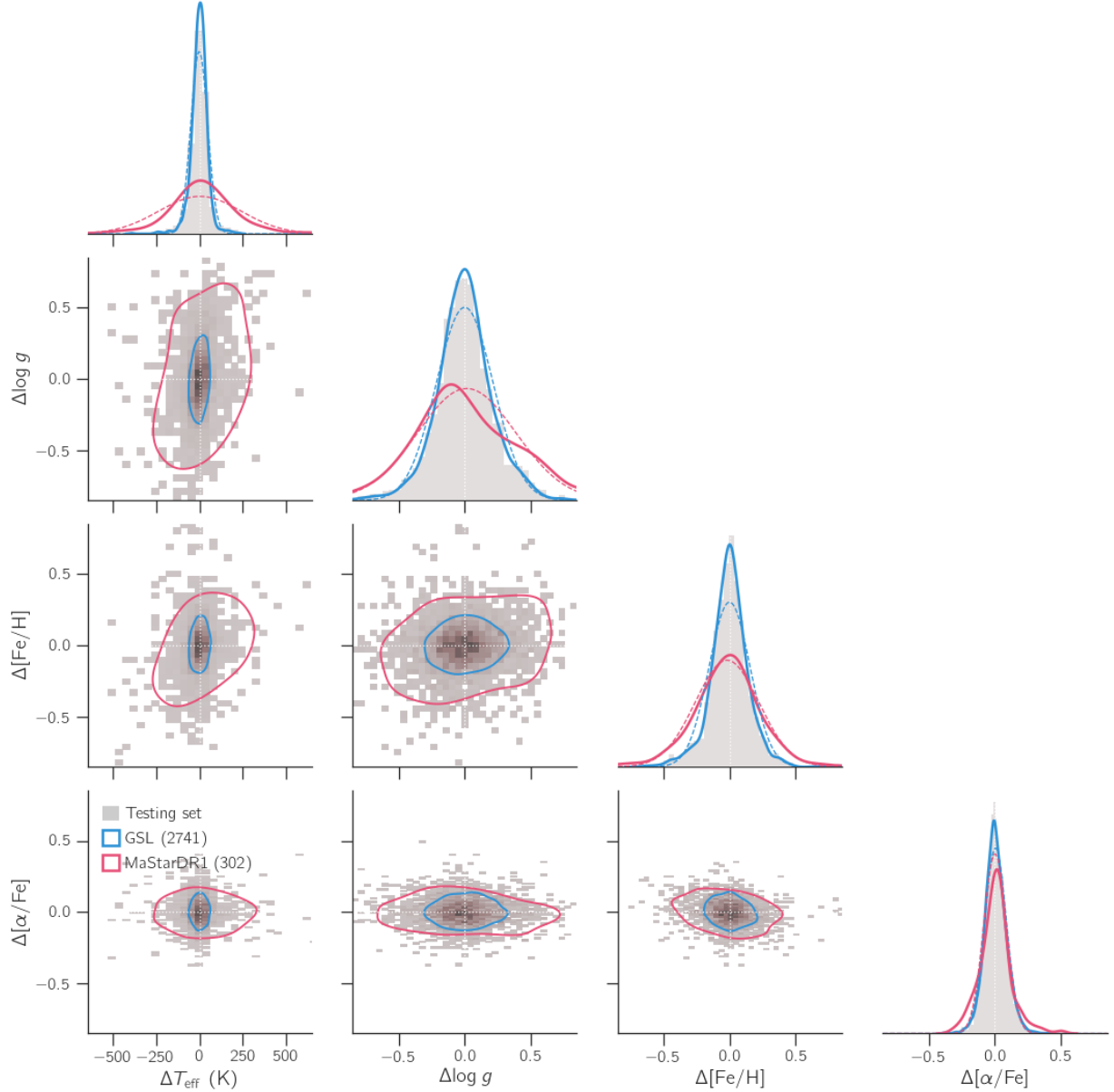


Figure 6. Joint distribution of residuals as defined in Eq. (3) in the parameter space. The results for the testing set is shown in grey. The residuals for the GSL and *MaStarDR1* subsets are shown in blue and red, respectively, like in Fig. 4. The univariate residuals are represented in the diagonal planes (histograms and solid lines). A Gaussian distribution with the intrinsic mean and standard deviation of the residuals is also represented (dashed lines) in the diagonal planes. The contours in the off-diagonal planes enclose 1σ of the probability distribution. We note the intrinsic errors from *MaStarDR1* are larger than our CoSHA internal errors and show larger deviation from the Gaussian behaviour. The lack of correlation in almost all projections of the residuals space suggests a striking lack of degeneracies. See text in § 4.2 for details.

rather consistent. These distributions disagree in their mean and standard deviation by at most ~ 0.18 and ~ 0.35 dex, respectively. The marginal distributions of $[\text{Fe}/\text{H}]$ and $[\alpha/\text{Fe}]$, on the other hand, show smaller discrepancies in their mean and standard deviation of at most ~ -0.01 and 0.15 dex, respectively, $[\alpha/\text{Fe}]$ being strikingly consistent.

The discrepancies in T_{eff} and $\log g$ show no trend with respect to the APOGEE estimate. Notwithstanding, both T_{eff} and $\log g$ show in fact a systematic discrepancy, whereby CoSHA seems to over-predict cooler and more dwarf stars than APOGEE. We expect the APOGEE error estimations to account for some of the observed discrepancy ($\Delta T_{\text{eff}} \sim 79$ K and $\Delta \log g \sim 0.05$, respectively). However, the remaining discrepancy is likely to

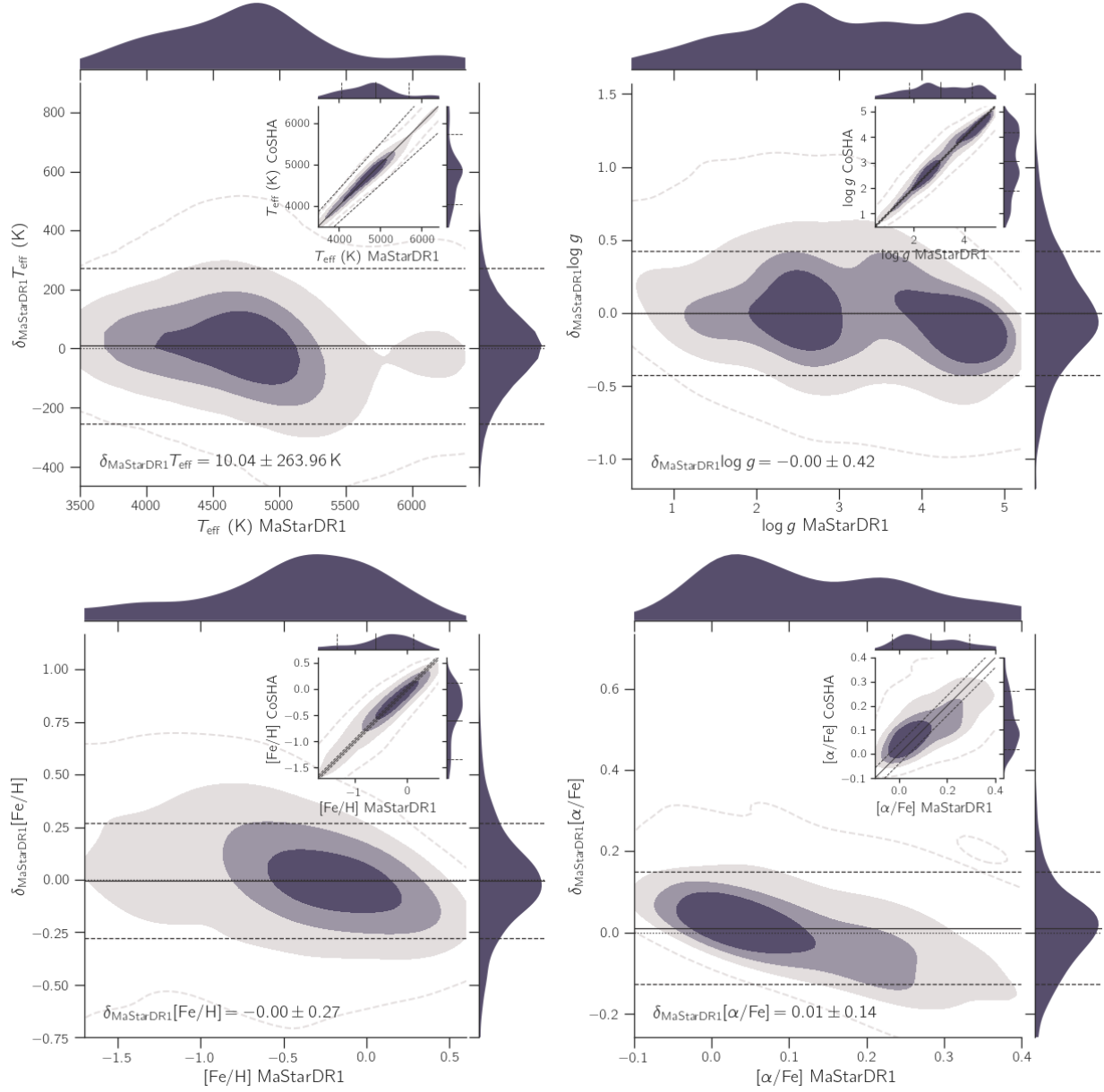


Figure 7. Distribution of the discrepancies defined in Eq. (4) between CoSHA and MaStarDR1 on the stellar properties T_{eff} , $\log g$, $[\text{Fe}/\text{H}]$ and $[\alpha/\text{Fe}]$. The color-coded contours represent the quartiles of the probability distribution. The dashed contours represent the 95% confidence region to illustrate how spread are these distributions. The marginal distributions are also shown (purple) along with the corresponding mean (solid line) and standard deviation (dashed lines). The dotted grey line represents a perfect consistency ($\delta\mathbf{Y} = 0$). A direct comparison between the stellar properties T_{eff} , $\log g$, $[\text{Fe}/\text{H}]$ and $[\alpha/\text{Fe}]$ retrieved in this study and MaStarDR1 is also shown in the inset axes. See text in § 4.3 for details.

have an origin in CoSHA. $[\text{Fe}/\text{H}]$ shows a mild discrepancy systematic and almost no trend with the values reported by APOGEE. $[\alpha/\text{Fe}]$, on the other hand, shows a trend between its discrepancy and the values reported for APOGEE: the higher the APOGEE estimates, the larger the discrepancy in the negative sense. It is worth mentioning that a similar trend was observed in the discrepancies with MaStarDR1. It is encouraging though, that the mean and standard deviation of the distribu-

tion of discrepancies are overall rather small. We think that this trend has its origin in our analysis as will be discussed in the next sections.

5. THE PARAMETER SPACE DISTRIBUTION

In the previous sections we explored the MaStar distribution of the stellar properties through its marginal distributions (c. f. Figs. 7 and 8). In Fig. 9 we introduce the final joint distribution of the stellar properties

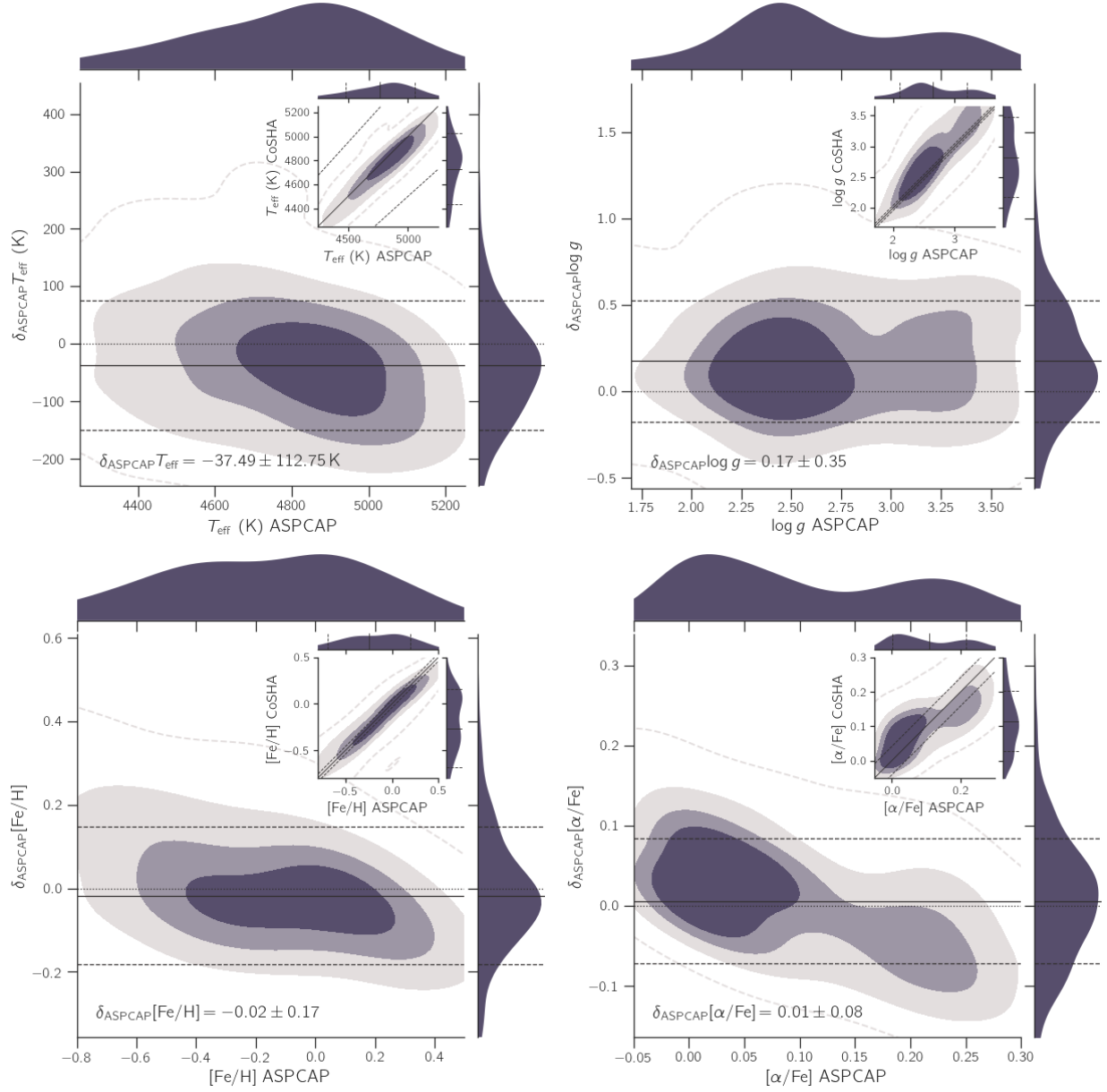


Figure 8. Similar to Fig. 7 but comparing our estimates to those derived by the APOGEE spectral analysis pipeline (ASPCAP). The systematic discrepancies with APOGEE are larger than those found with [MaStarDR1](#). In summary, CoSHA predicts systematically cooler and more dwarf stars and marginally Fe-poorer than APOGEE, with essentially no bias in the $[\alpha/\text{Fe}]$ estimates. See text in § 4.4 for details.

for the cleaned version of the MaStar library. The light purple distributions represent the raw estimates from our model. Since by construction these distributions are not a representative sample (see Fig. 3), this means that we cannot confidently validate our results using the currently known trends in the Milky Way (MW) provided by APOGEE. In order to solve for this issue, we implement the volume correction described in § 2.5. In Fig. 9 we show the volume corrected sample of MaStar parameters in dark purple. Interestingly, T_{eff} becomes flatter after correction, thus the peak around $T_{\text{eff}} \sim 6000 \text{ K}$ be-

comes less pronounced in favor of cooler stars. In the $\log g$ distribution dwarf stars ($\log g \sim 5$) become more relevant. The $[\text{Fe}/\text{H}]$ distribution in the raw MaStar distributions shows an oversampling of low iron abundance ($[\text{Fe}/\text{H}] \lesssim -1$) that is redistributed towards solar abundance after volume correction. $[\alpha/\text{Fe}]$ is perhaps the most unchanged distribution with a slight redistribution of $[\alpha/\text{Fe}] \sim 0.5$ towards solar values.

It is worth noticing that well-known distributions such as the $\log g$ versus T_{eff} and the $[\alpha/\text{Fe}]$ versus $[\text{Fe}/\text{H}]$ seem to follow the expected trends. In the following we

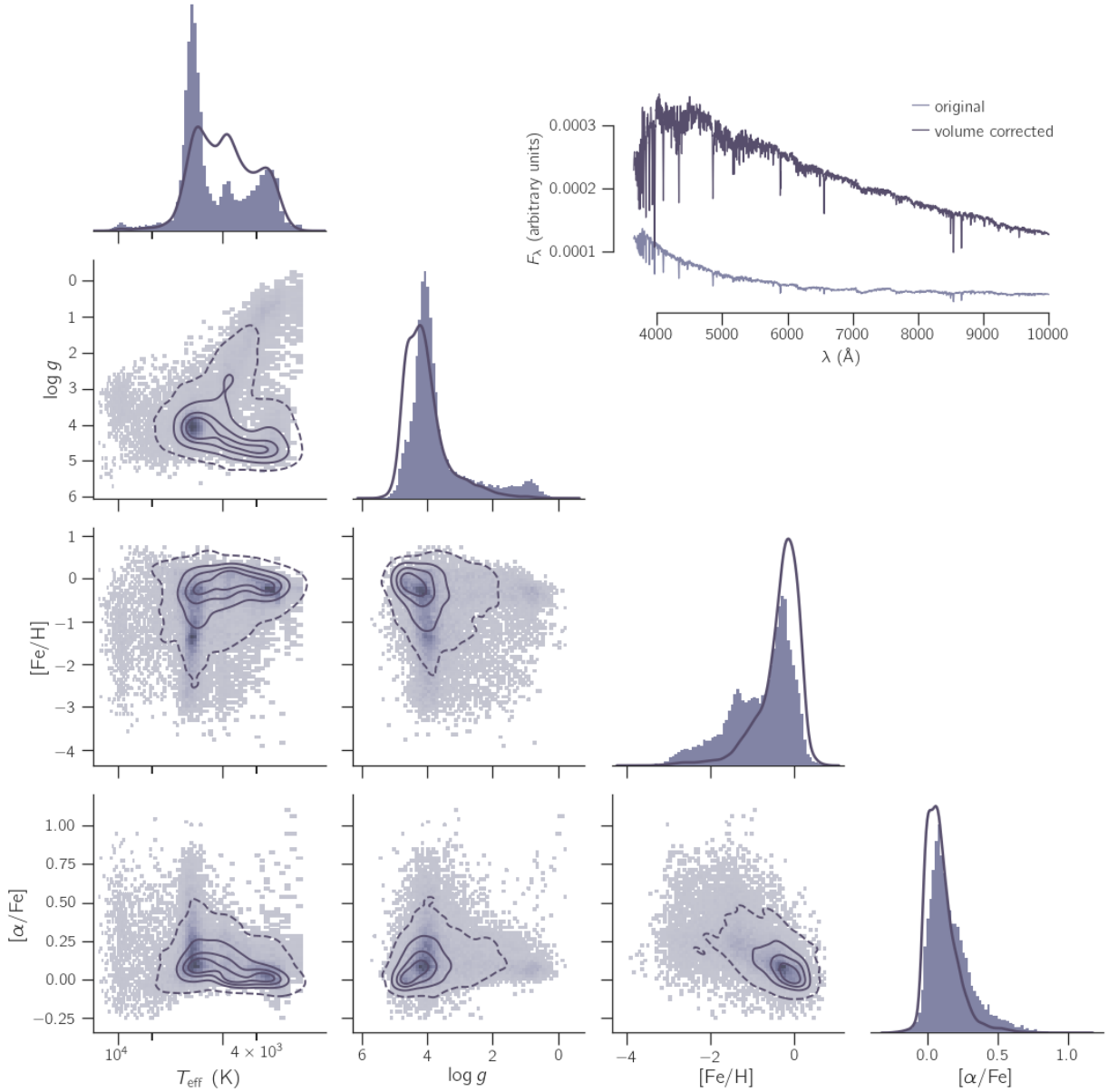


Figure 9. Similar to Fig. 4, the joint distribution of the stellar parameters for MaStar as estimated by CoSHA. In light and dark purple we show the original and the volume corrected distributions as explained in § 2.5, respectively. The contours are as in Fig. 5. The corresponding average spectrum of the MaStar library and the volume corrected one (inset axes). The in-homogeneity in the MaStar sampling of the parameter space become apparent. (i) T_{eff} becomes flatter after correction; (ii) $\log g$ is corrected for under-sampling of giant stars and; (iii) $[\text{Fe}/\text{H}]$ and $[\alpha/\text{Fe}]$ become more biased towards solar abundance patterns. See text in § 5 for details.

focus our attention in the analysis of these two physically relevant planes.

5.1. The $\log g$ versus T_{eff} distribution

Stars are known to follow a characteristic distribution in $\log g$ vs. T_{eff} plane, equivalent to the HR diagram. In this section we segregate this distribution into the dwarf stars ($\log g > 3.5$) and giant stars ($\log g \leq 3.5$), according to CoSHA estimates for the MaStar spectra. In

the previous sections we found that T_{eff} is the best estimated property. This makes sense since T_{eff} is traced by the overall shape of the stellar continuum, rather than narrow spectral features such as absorption lines and/or bands. $\log g$ on the other hand, is the most unreliable (from the internal tests) and inconsistent property (from the external tests). In summary we seem to predict a larger number of dwarf stars than they are predicted by other estimates (MaStarDR1 and APOGEE). This

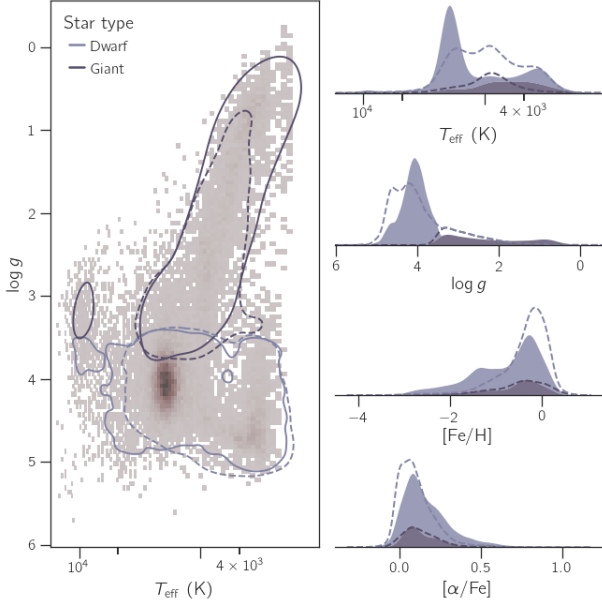


Figure 10. *left:* Distribution of $\log g$ vs. T_{eff} for the MaStar library (grey-scaled density). The contours enclose the 95% confidence region for the dwarf ($\log g > 3.5$; light purple) and the giant ($\log g \leq 3.5$; dark purple) stars. *right:* Distributions of T_{eff} , $\log g$, $[\text{Fe}/\text{H}]$ and $[\alpha/\text{Fe}]$ of dwarf and giant stars are also shown. Dashed distributions represent the volume corrected sample. See text in § 5.1 for details.

bias in the consistency is more important when comparing with APOGEE. We have to be careful on the interpretation of this bias though, since APOGEE is an IR spectroscopic survey. Therefore, it is inherently biased in favor of cool (K spectral type) sub-giant and giant stars. Under this rationale, it seems that our method is underestimating the number of this type of stars, regardless of their properties. In Fig. 10 we show $\log g$ vs. T_{eff} (left), whereby we split the MaStar stars classified using our method into dwarfs (light purple) and giants (dark purple). The segregation between dwarf and giant stars is more clear in T_{eff} distribution, giant stars being systematically cooler ($T_{\text{eff}} \sim 4000$ K) than dwarfs ($T_{\text{eff}} \sim 6000$ K), as expected. In $[\text{Fe}/\text{H}]$ both type of stars peak at around $[\text{Fe}/\text{H}] \sim -0.7$. However, giant stars seem to be systematically more iron rich than dwarfs. Furthermore, the iron-poor tail of the distribution is heavier for dwarf stars. The $[\alpha/\text{Fe}]$ abundance distribution seems to be more spread for dwarf stars, although both giant and dwarf stars peak at around solar α abundance pattern.

In $\log g$ vs. T_{eff} plane, the volume correction is increasingly important for giant stars: the uncorrected MaStar giant branch reaches $\log g \sim 0$ while the volume corrected giant branch is limited to $\log g > 1$. These stars are also systematically hotter than in the volume cor-

rected sample. Dwarfs, on the contrary, seem to be well represented in the MaStar library (at least in this plane). This is expected since all stars spend most of their lives in the main sequence, regardless of their initial physical properties. In the right panes the volume corrected T_{eff} distribution becomes flatter to fix the (under)sampling of cool ($T_{\text{eff}} < 5000$ K) stars. Giant stars on the other hand, become more biased towards $T_{\text{eff}} \sim 5000$ K. These type of stars are distributed in $[\text{Fe}/\text{H}]$ and $[\alpha/\text{Fe}]$ in the same fashion, regardless of the sample being volume corrected or not. Dwarf stars, instead, show solar chemical patterns after being volume corrected.

We have implemented a volume correction to compare the observed trends in the physical properties estimated from the MaStar spectra against what is known for the solar neighborhood. However, it is important to note that MaStar as a stellar library is not expected to be representative of the MW or any other galaxy stellar population, in principle. As a matter of fact our expectation is that MaStar to be a reliable stellar library to represent all physically plausible cases in nature. The intend of this expectation is to reproduce observations of the nearby and distant stellar populations and make robust inferences of their physical properties. None the less, given the observed distributions in Fig. 10, indicate that such expectations are still far from being fulfilled: the iron abundance and the α -enhancement are still biased towards solar chemical patterns and the most common spectral type of stars is G (like the Sun). This bias is hard to break and will require the development of more ambitious surveys such as the Milky Way Mapper (Kollmeier et al. 2017).¹

5.2. The $[\alpha/\text{Fe}]$ versus $[\text{Fe}/\text{H}]$ distribution

$[\alpha/\text{Fe}]$ vs. $[\text{Fe}/\text{H}]$ plane is a well characterized plane providing reliable estimates exist for a representative sample of stars, mostly in the MW (e. g. Hayden et al. 2015; Sharma et al. 2020), the MW neighborhood (e. g., Escala et al. 2020; Kirby et al. 2020), and integrated stellar populations (e. g., Walcher et al. 2016). The importance of this distribution becomes clear since its slope provides links to the past SFH of galaxies. Essentially, if all the stars were bound to evolve and yield their chemical products to the ISM in the same time-scales, the distribution of $[\alpha/\text{Fe}]$ would be collapsed towards $[\alpha/\text{Fe}] = 0$. That is, there would be no differential chemical evolution in the stellar populations (at least seen through these species). However, in reality all stars pollute the ISM with α -species (O, Ne, Mg, Si, S, Ar, Ca, and Ti) at short time-scales (< 1 Gyr), while the Fe-peak

¹ <https://www.sdss5.org/mappers/milky-way-mapper>.

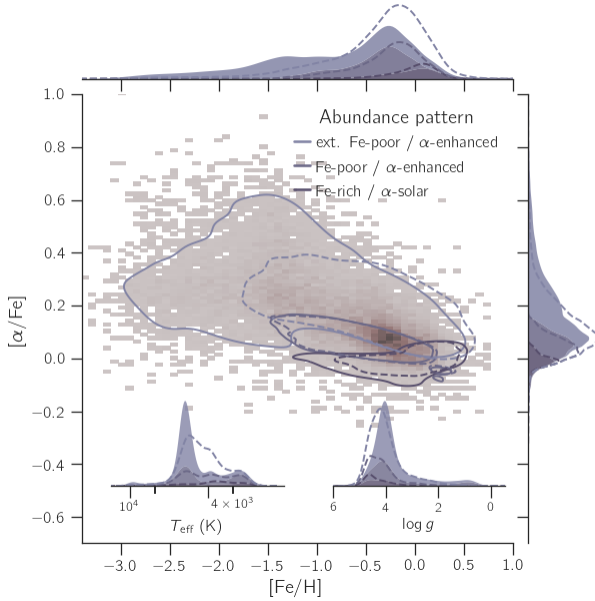


Figure 11. The $[\alpha/\text{Fe}]$ vs. $[\text{Fe}/\text{H}]$ distribution for the MaStar library (grey-scaled density). We split the distribution in three distinct components according to APOGEE-ASPCAP predictions: Fe-poor / α -enhanced (light purple), Fe-poor / α -rich (medium purple), and Fe-rich / α -solar (dark purple). The contours are drawn at the 95th percentile. The dashed distributions represent the volume corrected sample. The corresponding distributions for T_{eff} and $\log g$ are shown in the inset axis.

element enriching stars (SNe Ia progenitors) evolve in larger time-scales ($\gtrsim 1$ Gyr). Assuming a secular evolution (i. e., inflows/outflows of pristine/enriched gas are negligible), this reflects in some galaxies (and regions therein) as an Fe deficit in their most recent stellar populations, more commonly dubbed, as α -enhancement (Maraston et al. 2003).

In Fig. 11 we show the distribution of the MaStar properties in the $[\alpha/\text{Fe}]$ vs. $[\text{Fe}/\text{H}]$ plane (grey-scaled density). Stars are known to follow two characteristic sequences in this plane: one of high $[\alpha/\text{Fe}]$ which are mainly in the thick disk and one with solar abundance patterns ($[\text{Fe}/\text{H}] \sim 0$ and $[\alpha/\text{Fe}] \sim 0$) of stars mostly in the thin disk (e. g., Nandakumar et al. 2020). A separation of both stellar populations, the ones in the thin and the ones in the thick disk is not straightforward since some level of mixing is expected, regardless of the true origin of the thick disk. In order to disentangle these populations, we estimate the underlying probability distribution of observing a star at each point in this plane using a Extreme Deconvolution method (XD, Ivezić et al. 2019). In essence this algorithm fits a predefined set of Gaussian components in order to reproduce the observed distribution of stars. Since

the APOGEE results in the $[\alpha/\text{Fe}]$ vs. $[\text{Fe}/\text{H}]$ plane are used in plenty of studies as a reference, we implement the XD algorithm in the APOGEE distribution to reconstruct the probability density distribution, finding that it is well characterized by three components, dubbed: Fe-poor / α -enhanced, Fe-poor / α -rich and Fe-rich / α -solar. In Fig. 11 we show the Gaussian components evaluated in the MaStar properties predicted by COSHA as contours enclosing the 95% of the probability (solid lines). The stars characterized by Fe-rich and α -solar in the MaStar library extend also towards Fe-poor stars, while the other two types of abundance patterns occupy almost the same loci as in the APOGEE distributions. The distributions of T_{eff} and $\log g$ (insets) show some interesting insights about the type of stars dominating these populations. Fe-poor and α -enhanced patterns clearly dominate the prominent peak around $T_{\text{eff}} \sim 6000$ K, which are mostly dwarf/turn-off stars. Interestingly, most giant stars in MaStar ($\log g \lesssim 0$) are also characterized by these abundances. On the other hand, in hotter dwarf stars around $T_{\text{eff}} \lesssim 12000$ K and $\log g \sim 4 - 3$, Fe-poor and Fe-rich abundance patterns become more relevant. The volume corrected versions of these same distributions (dashed) move towards solar abundance patterns, with the distribution of α -enhanced stars being changed the most, as expected.

5.3. Spatial distributions

In Fig. 12 we show the spatial distribution in the z direction of the galactic plane, for the stars in MaStar (purple) and the APOGEE (grey) surveys. In the top panels we show the matched subset of (~ 400) stars between both surveys. In all the panels the expected trends appear whereby stars become more Fe-poor and α -enhanced towards the thick disk (higher $|z|$), and they present abundances more similar to the solar one towards the thin disk. In the bottom panels we compare the full samples to see if the aforementioned trends remain in MaStar. Although the scatter is clearly larger in this case, the trends are still statistically significant. It is reassuring that we retrieve these trends using COSHA since, in principle, the training process is unaware of the spatial distribution of the stars. This result reinforces the robustness of our COSHA, already drawn from the internal and external tests (c. f., § 4).

6. SUMMARY AND CONCLUSIONS

We present the novel Code for Stellar properties Heuristic Assignment (COSHA) to estimate atmospheric parameters from the MaStar stellar optical spectral energy distributions, namely: T_{eff} , $\log g$, $[\text{Fe}/\text{H}]$ and $[\alpha/\text{Fe}]$. COSHA implements a machine learning (ML)

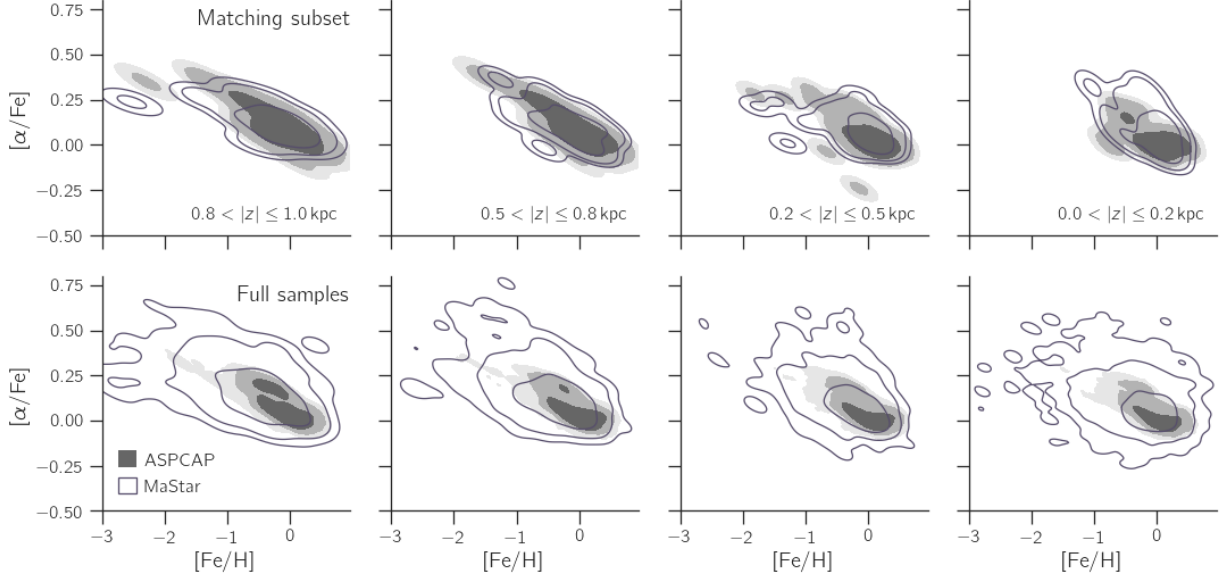


Figure 12. Spatial distribution of the MaStar stars (purple) in the $[\alpha/\text{Fe}]$ vs. $[\text{Fe}/\text{H}]$ plane, segregated by the vertical distance to the MW disk plane, z . As a reference we use the corresponding distribution for APOGEE-ASPCAP (grey). In the top panels we compare only the matched subset of stars between the two surveys and in the bottom panels we compare the trends found in the full samples for both surveys. In the top panels it is appreciated that MaStar and APOGEE are statistically indistinguishable from each other, for any vertical distance. The full samples are still compliant, albeit the larger scatter in MaStar, with the expected trends: stars become more Fe-poor and α -enhanced towards the thick disk, whilst in the thin disk stars with solar abundances dominate. See text in § 5.3 for details.

approach named Gradient Tree Boosting (GTB) which consists in training a predefined number of decision trees sequentially, each improving its predecessor. The main strength of this approach is that it is easier to interpret its results and easier to scale than more commonly used approaches such as artificial neural networks.

For the training and testing samples we used a combination of empirical (MaStarDR1) and theoretical (GSL) libraries. Both have advantages and disadvantages that were explained (see § 2). Despite of them we were able to use train a model providing reliable results. Based on the internal tests (i. e., comparing the input with the output) using the testing subset, an overall performance of CoSHA of: $\Delta T_{\text{eff}} \sim -2 \pm 75 \text{ K}$, $\Delta \log g \sim 0.004 \pm 0.249$, $\Delta [\text{Fe}/\text{H}] \sim -0.007 \pm 0.169$ and $[\alpha/\text{Fe}] \sim 0.004 \pm 0.088$. Moreover, the performance of CoSHA on the segregated MaStarDR1 and GSL subsets showed a systematically more imprecise estimate of the physical properties on the former, even after the internal errors from CoSHA were removed. The fact that the errors on the GSL properties are smaller than in the MaStarDR1 points towards an origin in the MaStarDR1 subset itself. We reckon several possibilities: a smaller (than GSL) statistical sample, instrumental noise and/or internal errors introduced by the different methods adopted by MaStarDR1. None of these issues

are present in the GSL subset. The main results can be summarized as follows:

- We found no statistically significant difference on the distributions of the predicted parameters between the values derived by CoSHA and those published by MaStarDR1. The systematic and random discrepancy between such distributions are: $\delta T_{\text{eff}} \sim 15 \pm 325 \text{ K}$, $\delta \log g \sim 0.01 \pm 0.43$, $\delta [\text{Fe}/\text{H}] \sim -0.01 \pm 0.27$ and $\delta [\alpha/\text{Fe}] \sim 0.01 \pm 0.14$. Most of the parameters show no trend between the discrepancy and the reference MaStarDR1's values, except for $[\alpha/\text{Fe}]$. This parameter becomes more increasingly more inconsistent (with respect to MaStarDR1) for higher values of $[\alpha/\text{Fe}]$.
- The comparison between CoSHA and APOGEE-ASPCAP estimates on a subset of (~ 400) stars in common between both surveys, revealed systematic discrepancies comparable to those in the previous item: $\delta T_{\text{eff}} \sim -45 \pm 101.28 \text{ K}$, $\delta \log g \sim 0.18 \pm 0.35$, $\delta [\text{Fe}/\text{H}] \sim -0.01 \pm 0.15$ and $\delta [\alpha/\text{Fe}] \sim 0.00 \pm 0.08$. The errors reported by ASPCAP can only account for a fraction of the total systematic discrepancy. We interpreted this to mean that CoSHA systematically predicts slightly cooler and more giant stars than APOGEE. The trend found for $[\alpha/\text{Fe}]$ in the MaS-

tarDR1 discrepancy remains present when comparing to APOGEE, although with a less steep slope. We interpreted this finding as an evidence that this trend is most likely to be originated in CoSHA.

- We predicted the atmospheric properties of the entire (cleaned) MaStar stellar spectra using CoSHA and characterized the resulting distribution in the parameter space: the most common stars in the library seem to have around $T_{\text{eff}} \sim 6000$ K (similar to the Sun's) and being close to the turn-off point. The iron abundance is slightly sub-solar and the α -elements abundance relative to iron is slightly above the solar value. This result highlights a deficit of thin disk stars in MaStar, according to CoSHA predictions. The volume-corrected distributions support these conclusions.
- In order to further characterize the MaStar stellar parameter distribution, we analyzed $\log g$ vs. T_{eff} plane by segregating the stars into dwarfs ($\log g > 3.5$) and giants ($\log g \leq 3.5$). We found the expected trends: the bulk of dwarf stars (around the turn-off point) are the hotter stars ($T_{\text{eff}} \gtrsim 6000$ K), while giant stars spread out below $T_{\text{eff}} \sim 5000$ K and around $T_{\text{eff}} \sim 4000$ K. The smaller peak in temperature ($T_{\text{eff}} \lesssim 4000$ K) of dwarf stars corresponds to the lower main-sequence stars. The iron and α -elements abundance suggest that MaStar has an under-sampling of non-solar abundance stars, a more deficit more important in the giant stars. However, we cannot rule out that this could be due to the in-homogeneous sampling of parameter space in the GSL for this particular type of stars. The volume corrected versions of these distributions suggest that the solar vicinity can be characterized by (i) flattened distributions of temperature for dwarf stars, and giant stars peaking around $T_{\text{eff}} \sim 5000$ K; (ii) a systematic over/under-sampling of dwarf/giant stars; and (iii) more solar-like abundance stars.
- Likewise, we characterized $[\alpha/\text{Fe}]$ vs. $[\text{Fe}/\text{H}]$ plane by dividing the MaStar stars into Fe-poor / α -enhanced, Fe-poor / α -rich and Fe-rich / α -solar abundance patterns, according to APOGEE-ASPCAP predictions. We find that: (i) stars characterized by Fe-poor / α -enhanced are mostly solar-like spectral types; (ii) these stars span a wide range of Fe-abundance, reaching $[\text{Fe}/\text{H}] \sim -1.5$; (iii) a smaller fraction of stars with these abundance patterns are cool $T_{\text{eff}} \sim 4000$ K

giants; (iv) an even smaller fraction are the hottest stars in the library with $T_{\text{eff}} \sim 12000$ K. In general, stars with iron and α abundances closer to the solar one tend to be around or cooler than $T_{\text{eff}} \sim 6000$ K dwarf stars. The volume correction tends to affect mostly non-solar abundance stars.

- The spatial distribution of the MaStar stars in $[\alpha/\text{Fe}]$ vs. $[\text{Fe}/\text{H}]$ for the matched subset of stars in the APOGEE survey reveals an encouraging agreement with the known trends in the z direction of the Galactic plane. The comparison of the full MaStar and APOGEE samples reveals the same trends.

In summary we have assigned parameters to the MaStar stellar library using a simple heuristic, non-exhaustive, machine learning approach to predict the atmospheric parameters T_{eff} , $\log g$, $[\text{Fe}/\text{H}]$ and $[\alpha/\text{Fe}]$ from the optical spectra of ~ 22 k unique stars. Our method, dubbed CoSHA, not only allowed to expand the state-of-the-art empirical libraries in size, but also in dynamical range of the parameter space. The robustness of CoSHA predictions is clear since without any information about the spatial distribution of the physical properties of the stars in the library, it reproduces the known trends, at least to an statistical level. The version of MaStar presented in this work will grow our ability to analyze resolved and unresolved stellar populations with a precision without precedents.

We thank CONACYT FC-2016-01-1916 and CB-285080 projects and PAPIIT IN100519 project for support on this study. GB acknowledges financial support from the National Autonomous University of México (UNAM) through grant DGAPA/PAPIIT IG100319 and from CONACyT through grant CB2015-252364. LC thanks the founding through the PAPIIT IN103820 project. J.B-B acknowledges support from the grant IA-100420 (DGAPA-PAPIIT, UNAM) and funding from the CONACYT grant CF19-39578.

Funding for the Sloan Digital Sky Survey IV has been provided by the Alfred P. Sloan Foundation, the U.S. Department of Energy Office of Science, and the Participating Institutions.

SDSS-IV acknowledges support and resources from the Center for High Performance Computing at the University of Utah. The SDSS website is www.sdss.org.

SDSS-IV is managed by the Astrophysical Research Consortium for the Participating Institutions of the SDSS Collaboration including the Brazilian Participation Group, the Carnegie Institution for Science, Carnegie Mellon University, Center for Astrophysics

— Harvard & Smithsonian, the Chilean Participation Group, the French Participation Group, Instituto de Astrofísica de Canarias, The Johns Hopkins University, Kavli Institute for the Physics and Mathematics of the Universe (IPMU) / University of Tokyo, the Korean Participation Group, Lawrence Berkeley National Laboratory, Leibniz Institut für Astrophysik Potsdam (AIP), Max-Planck-Institut für Astronomie (MPIA Heidelberg), Max-Planck-Institut für Astrophysik (MPA Garching), Max-Planck-Institut für Extraterrestrische Physik (MPE), National Astronomical Observatories of China, New Mexico State University, New York University, University of Notre Dame, Observatório Nacional / MCTI, The Ohio State University, Pennsylvania State University, Shanghai Astronomical Observatory, United

Kingdom Participation Group, Universidad Nacional Autónoma de México, University of Arizona, University of Colorado Boulder, University of Oxford, University of Portsmouth, University of Utah, University of Virginia, University of Washington, University of Wisconsin, Vanderbilt University, and Yale University.

Software: python (Van Rossum & Drake Jr 1995; Van Rossum & Drake 2009), numpy (Oliphant 2006), scipy (Virtanen et al. 2020), matplotlib (Hunter 2007), seaborn (Waskom et al. 2017), scikit-learn (Pedregosa et al. 2011b), astroML (Vanderplas et al. 2012), astropy (Price-Whelan et al. 2018), astroquery (Ginsburg et al. 2019), dust-extinction (<https://pypi.org/project/dust-extinction/>), dustmaps (Green 2018)

APPENDIX

A. MACHINE LEARNING: A BRIEF INTRODUCTION

Machine Learning (ML) can be comprised into a series of statistic and calculus algorithms combined in order to uncover patterns in a data set, without making strong assumptions on the shape of those patterns. The process of uncovering such structures in a given data set is the so called *training* process and its result is the model itself, which can then used to make predictions on new observations. In broad terms, ML algorithms can be classified, regarding the training process, into supervised, semi-supervised, unsupervised and reinforcement learning. In this study we implement the two most common ones: supervised and unsupervised algorithms. We expand on those in the following.

Supervised learning: The main goal of these algorithms is to reveal the shape of the relationship between a given data set arranged in a matrix \mathbf{X} and a set of variables arranged in matrix \mathbf{Y} , such that for each record (sample) in \mathbf{X} corresponds a record in \mathbf{Y} . The supervised character of these algorithms comes from the fact that the mentioned relationship is learned from a controlled sample, for which the target variable, \mathbf{Y} is well-known. Examples of these algorithms are classifications and regressions.

Unsupervised learning: In this instance no knowledge is required about the variables \mathbf{Y} , instead the learning process consists in finding patterns among the variables in \mathbf{X} . Examples of these algorithms are clustering.

B. MODEL EVALUATION

In this section we evaluate the consistency in the parameter space between APOGEE-CANNON and Gaia and our method, for the sake of completeness.

B.1. Consistency with the CANNON

The APOGEE spectra has also been analyzed with the CANNON (Ness et al. 2015). The CANNON implements a data-driven method (similar to ML), which during the training stage fits a set of coefficients that describe the relation between the spectral space and the parameter space through a generative model. Such model is described as a second order polynomial function of the parameter space. In this section we compare the performance of the CANNON on the APOGEE subset of stars in common with the MaStar library, with that of CoSHA. In Fig. 13 we show the consistency between the APOGEE-CANNON and CoSHA. The similarity of these discrepancy distributions with those of APOGEE-ASPCAP is evident all across the parameter space. This in turn reveals that the CANNON is highly consistent with ASPCAP, at least for the APOGEE subset explored in this results. A full comparison between these two methods is beyond the scope of the current study, however the reader may refer to Nandakumar et al. (2020) for a similar consistency test.

B.2. Consistency with Gaia

Even though the Gaia survey is not focused in estimating the stellar parameters discussed in this study, they do indeed have to assume some of these properties ($\log g$ and $[\text{Fe}/\text{H}]$) in order to estimate other parameters of their interest

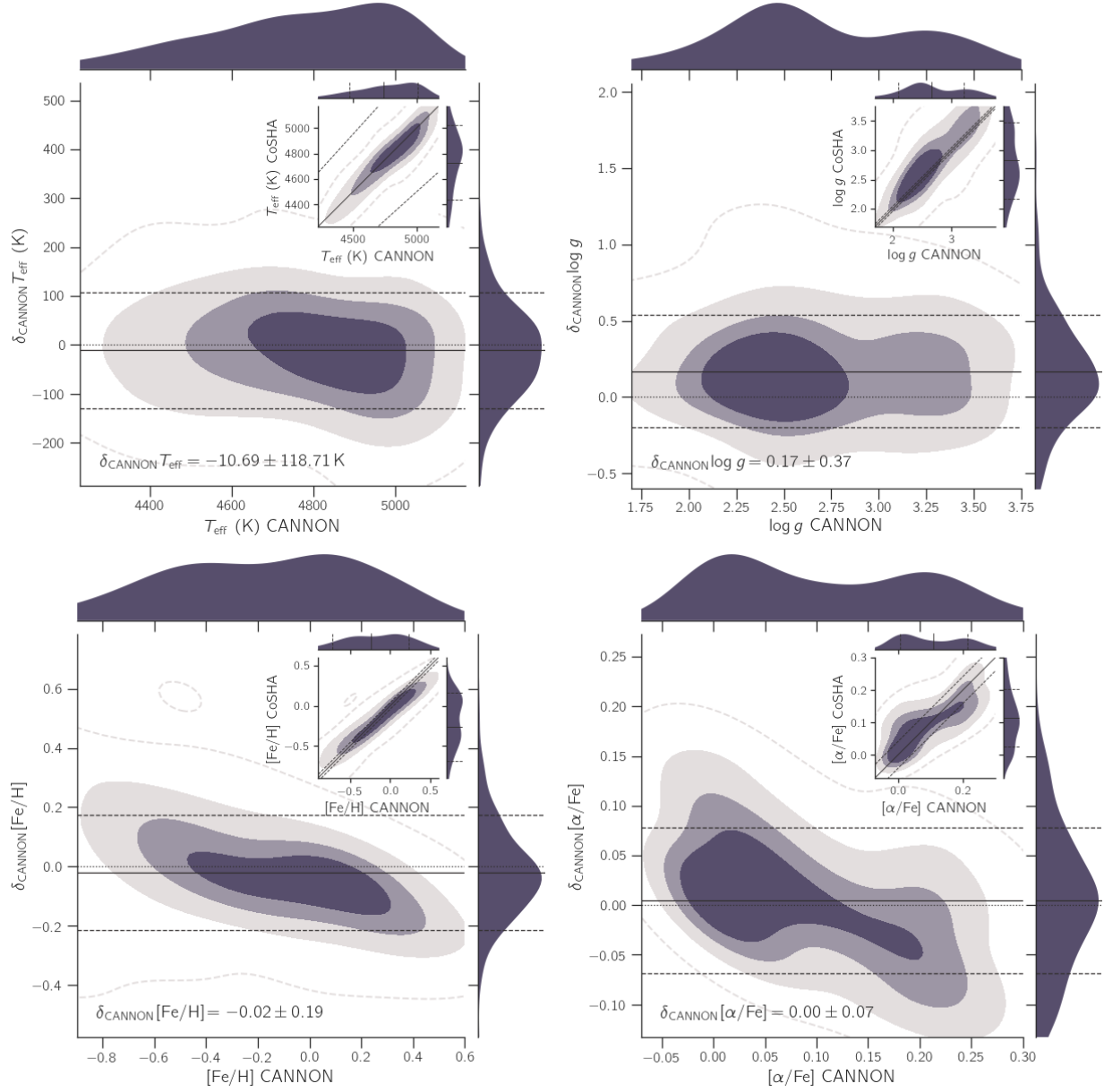


Figure 13. Similar to Fig. 8 but comparing with the APOGEE-CANNON estimates. The consistency between the APOGEE-CANNON and CoSHA estimates is statistically indistinguishable from that of APOGEE-ASPCAP.

(e. g., T_{eff}). In this section we compare both the values of the properties assumed by Gaia and the ones estimated by CoSHA for the cleaned MaStar library. Hence, even though Gaia’s estimates may be coarse, we at least have a statistical leverage to work with, as opposed to our previous tests that were limited to a subset of stars. In Fig. 14 we show such comparison of the T_{eff} , $\log g$ and the $[\text{Fe}/\text{H}]$ between Gaia’s and our estimates. We follow the same convention/notation as in Fig. 7. As expected the most consistent property turns out to be the T_{eff} . This is probably due to the fact that the photometric system adopted in by Gaia allows for accurate estimations of this property for most stars. We report absolute value discrepancies in the mean and the standard deviation of the distributions of ~ 80 and -81 K , respectively. The $\log g$ and $[\text{Fe}/\text{H}]$ properties, on the other hand, exhibit more discrepant behaviours, being $\log g$ the most inconsistent property all across its domain. In particular there is a tendency of our method to over estimate the number of giant stars ($\log g \geq 4$) with respect to Gaia’s predictions, whilst main-sequence stars ($\log g \sim 3$) according to Gaia, are found preferentially in two loci around $\log g \sim 1$ and ~ 4.5 , in our estimates. Since the spectral features relevant to the $\log g$ are mostly narrow features, estimates based on Gaia’s photometry are bound

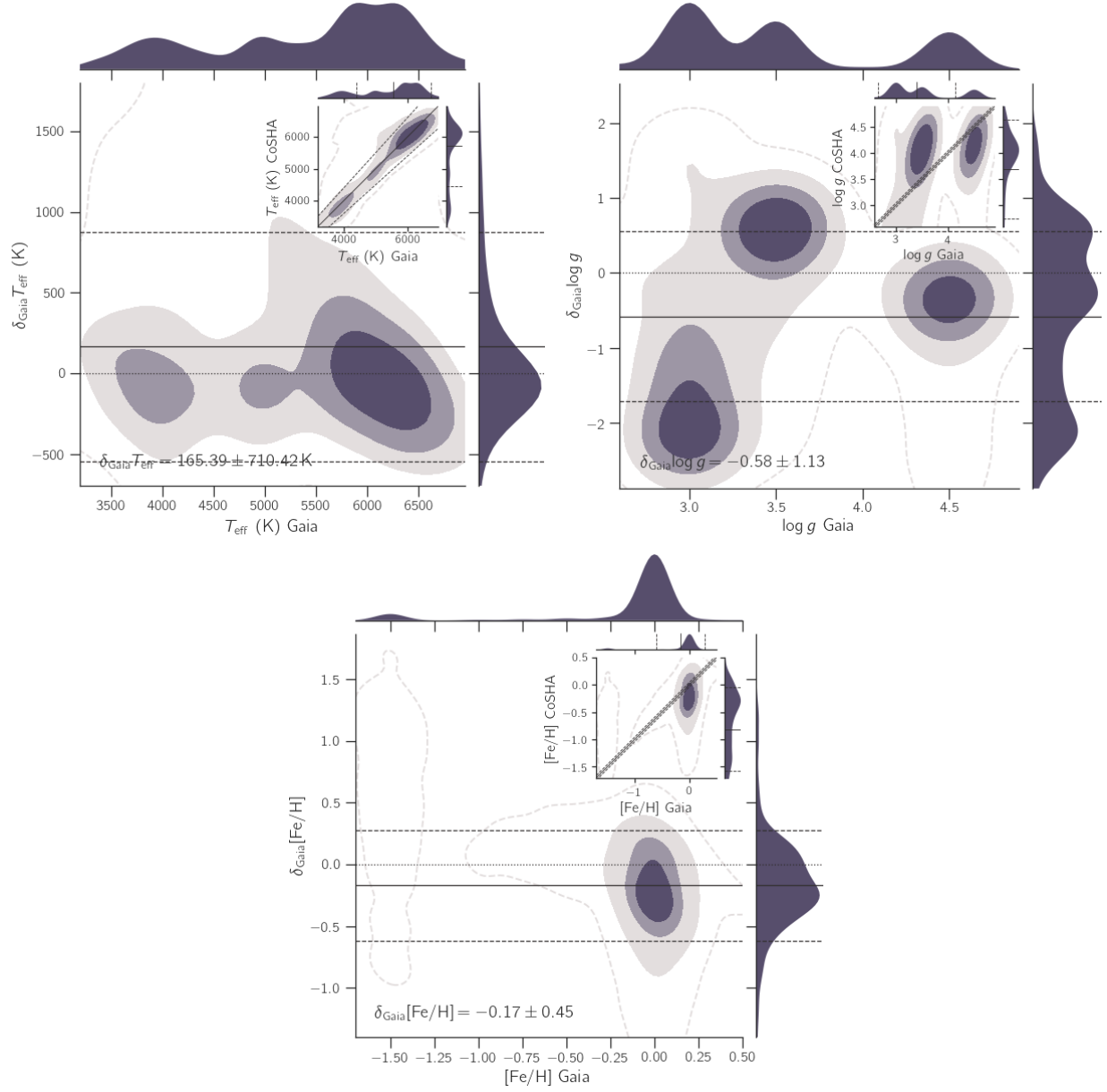


Figure 14. Similar to Fig. 7 but comparing with the Gaia estimates. T_{eff} is the most consistent property, with most of the sample within $\pm 10\%$ consistency. $\log g$ and $[\text{Fe}/\text{H}]$ on the other hand, show large inconsistencies, specially the former property. We should note though, that Gaia photometric system is not suitable to constrain these properties to accuracy comparable to spectroscopic data. See text in § B.2 for details.

to be unreliable. The consistency in the $[\text{Fe}/\text{H}]$ property seems to be less catastrophic, with both distributions having a discrepancy in their mean and standard deviation of ~ -0.67 and ~ 0.28 dex, respectively. In order to confidently rule out any possibility that our method is introducing the $\log g$ trends, we rely on the external tests.

C. COMPARISON WITH OTHER STELLAR LIBRARIES

In this section we explore to what extend the MaStar library as analyzed by CoSHA improves the sampling of the parameter space upon previous empirical libraries. This is not meant to be an exhaustive exploration, but merely a comparison with widely used stellar libraries. For this purpose we choose the IndoUS (Valdes et al. 2004) and MILES (Sánchez-Blázquez et al. 2006; Cenarro et al. 2007) stellar libraries. Since we both these libraries are freely available to download, we analyze the corresponding spectra using CoSHA and then compared the resulting parameter

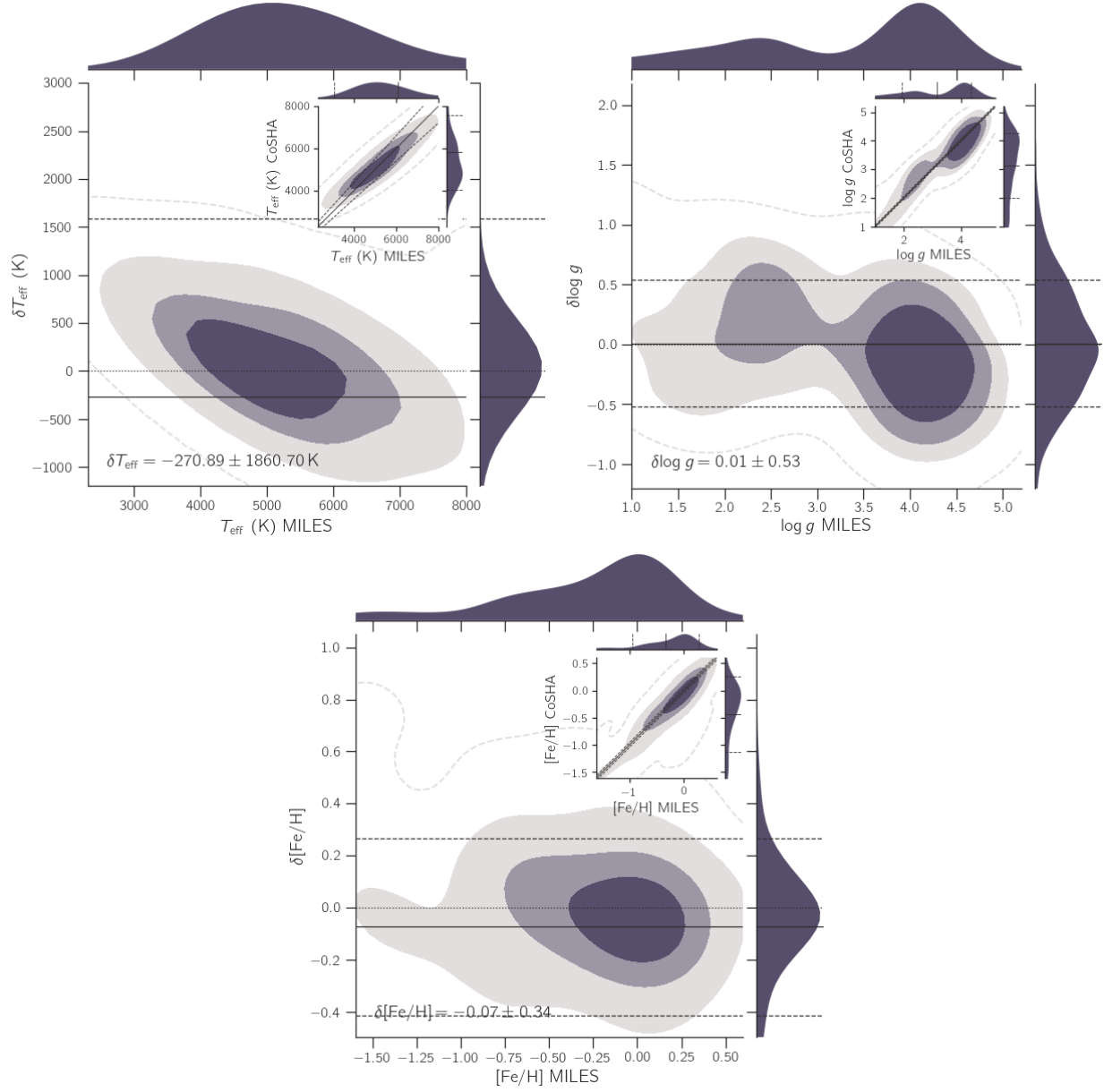


Figure 15. Similar to Fig. 7 but comparing CoSHA estimates for the MILES spectra and those distributed with the library.

distribution with the one distributed with those libraries. There is a caveat though: the wavelength range coverage. As a matter of fact, MaStar, MILES and IndoUS do not have the same coverage of the optical wavelength range, nor the same sampling and resolution. We use the same pre-processing procedure described in § 2.4. We fill in the missing pixels in MILES ($\lambda \sim 7,500 - 10,000 \text{ \AA}$) and in IndoUS ($\lambda \sim 9,500 - 10,000 \text{ \AA}$) using as a reference the MaStar spectra. We compared the performance of CoSHA with and without filling in the missing pixels in MILES and IndoUS and found a considerable improvement in the parameter space after extending the spectral range in those libraries. Another difference is that both this libraries have no publicly available $[\alpha/\text{Fe}]$ estimate (however see Knowles et al. 2021; Coelho et al. 2020, in the case of MILES), hence we limit our consistency tests to T_{eff} , $\log g$ and $[\text{Fe}/\text{H}]$ only.

C.1. MILES Library

In Fig. 15 we show the consistency between the parameters estimated with CoSHA for the MILES stellar spectra and those distributed with the library. There is a large inconsistency in T_{eff} of $\sim -270 \pm 1860$ K. In $\log g$ and $[\text{Fe}/\text{H}]$,

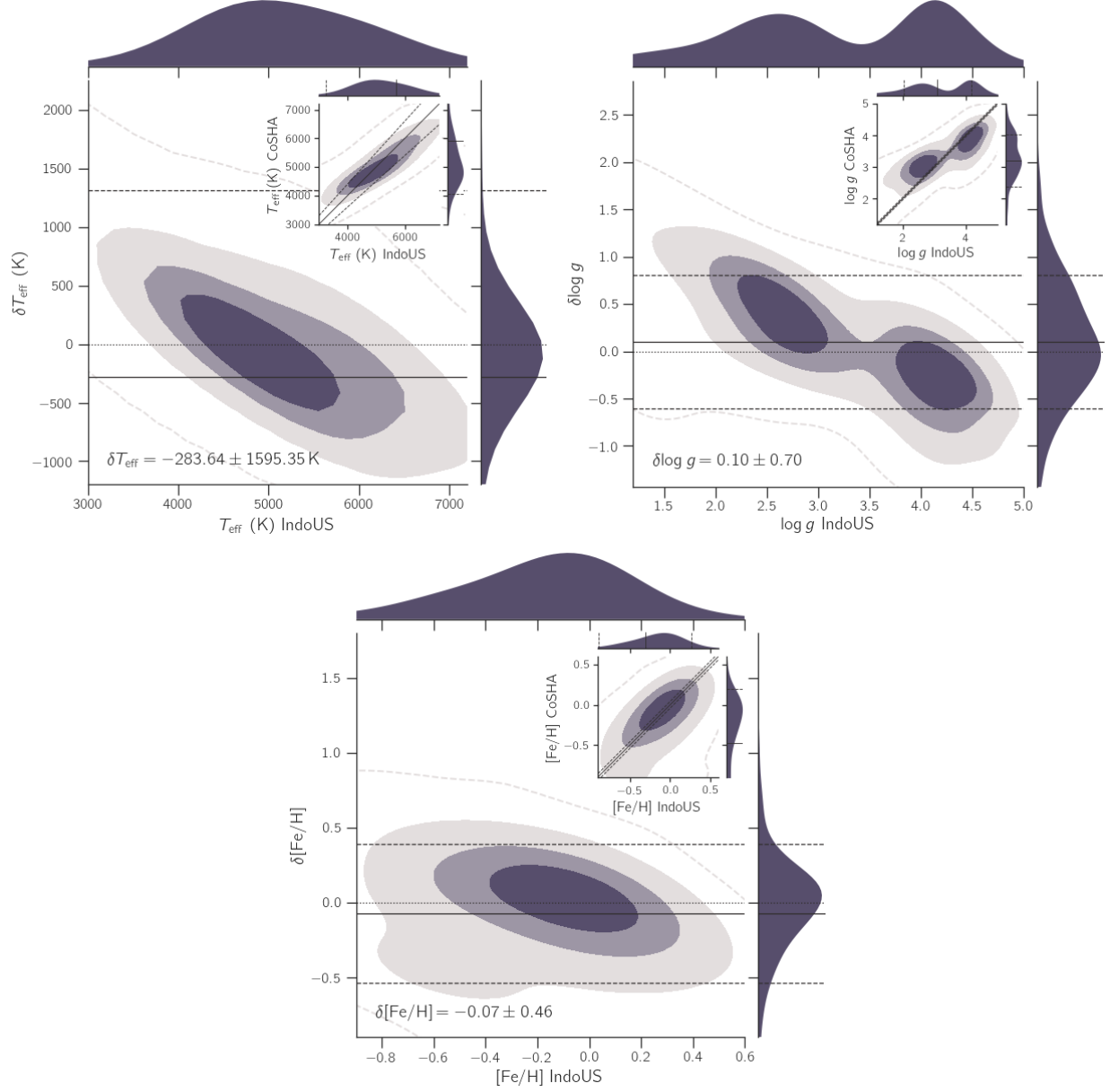


Figure 16. Similar to Fig. 15 but for IndoUS. T_{eff} and $\log g$ are the most inconsistent parameters, showing trends that suggest a limitation in the extrema of the parameter space for CoSHA.

even though the systematic discrepancy is small ~ 0.01 and ~ 0.07 dex respectively, the statistical dispersion around that systematic is rather large, with ~ 0.53 and ~ 0.34 dex, respectively. The trend observed in δT_{eff} with respect to the MILES value, along with the large dispersion may indicate a limitation in CoSHA to predict temperatures at the MILES extrema.

C.2. IndoUS Library

In Fig. 16 we show the consistency distribution between CoSHA and IndoUS. Similar to the case of MILES we find that δT_{eff} and $\delta \log g$ have trends with the IndoUS value, suggesting a limitation in the parameter space coverage by CoSHA. In particular, T_{eff} has a similar to MILES inconsistency trend, but in $\log g$ IndoUS inconsistency is worse. The level of agreement in $[\text{Fe}/\text{H}]$ is again similar to that found for MILES.

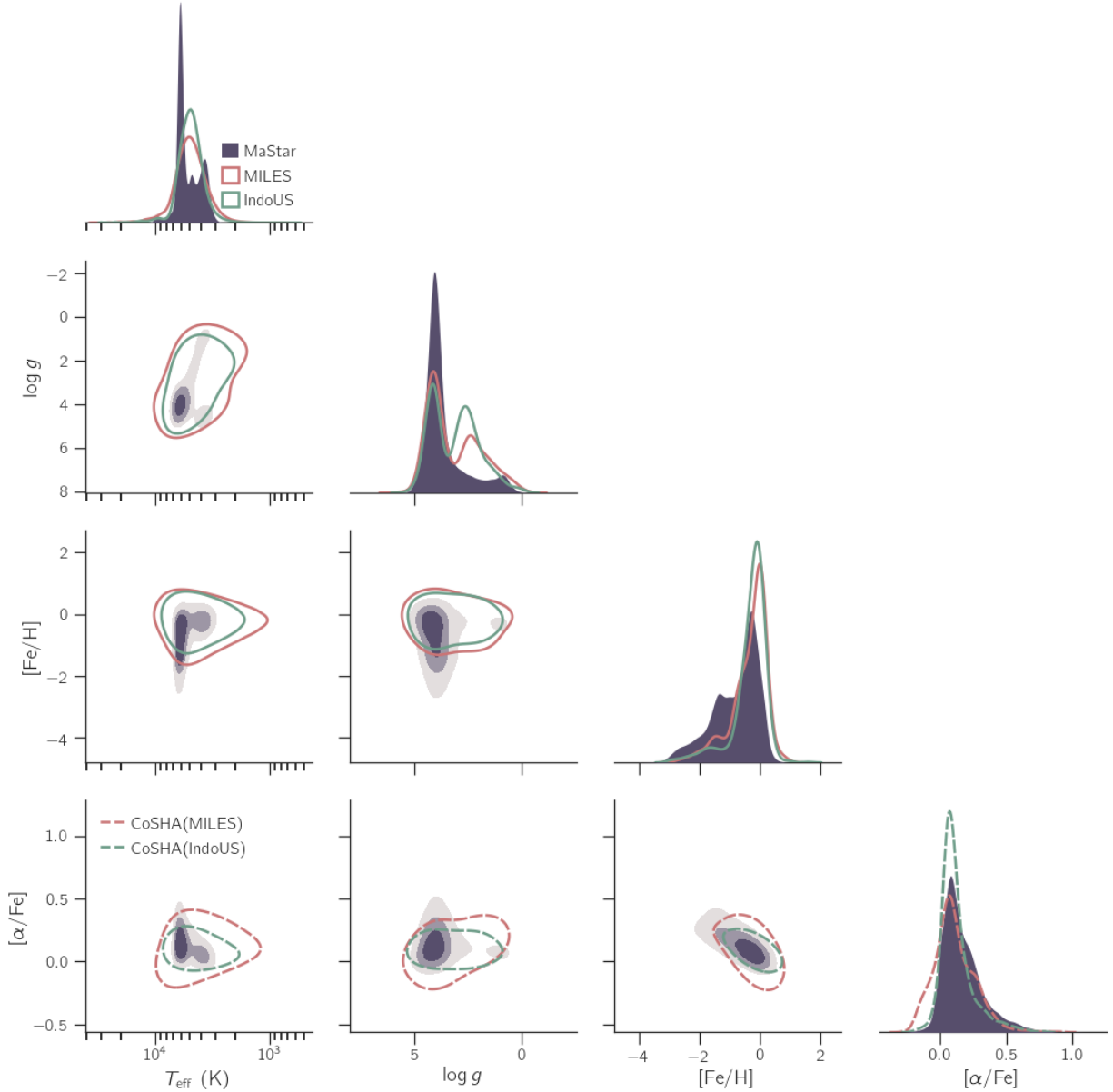


Figure 17. Comparison between MILES (pink), IndoUS (green) and MaStar (purple) parameter coverage. MaStar contours enclose the 25%, 50% and 75%. MILES and IndoUS enclose the 75%. MaStar is only superseded by MILES and IndoUS in the high effective temperature side of the parameter space, whilst in $\log g$ all libraries have similar coverage and in $[\text{Fe}/\text{H}]$ MaStar extends the lower metallicity extreme by one order of magnitude. We show the $[\alpha/\text{Fe}]$ distributions as computed by CoSHA (dashed lines) for completeness. Again all libraries share a similar coverage in this parameter.

C.3. Space parameter coverage

In Fig. 17 we show the parameter space coverage of the MILES, IndoUS and MaStar libraries, for comparison purposes. MILES, IndoUS and MaStar lowest contour enclose 75% of the density distribution. For completeness we show the $[\alpha/\text{Fe}]$ distributions of MILES and IndoUS computed using CoSHA (dashed distributions). Clearly MILES and IndoUS span a wider range in T_{eff} , reaching to $\sim 30,000$ K as opposed to 12,000 K for MaStar. In $\log g$ all libraries have similar coverage, with the MaStar extending the limits only marginally. In $[\text{Fe}/\text{H}]$ MaStar extends the lower end of the distribution, reaching down to ~ -4 dex as opposed to ~ -3 dex for MILES and IndoUS. We recall that the limitations in the MaStar parameter coverage is likely to have its origin in the training set and can be lifted by including hotter stars. Albeit such weaknesses, the version of the MaStar presented throughout this study has an

important advantage: since MaStar has over one order of magnitude more stars than these stellar libraries, it provides the best sampling of the parameter to date by any empirical library.

REFERENCES

- Arenou, F., Luri, X., Babusiaux, C., et al. 2018, *Astronomy and Astrophysics*, 616, 1
- Bailer-Jones, C. A. L., Rybizki, J., Fouesneau, M., Mantelet, G., & Andrae, R. 2018, arXiv, 58, 58. <https://iopscience.iop.org/article/10.3847/1538-3881/aacb21>
- Barbuy, B., Erandes, H., Souza, S. O., et al. 2021, *Astronomy & Astrophysics*, 648, A16. <https://www.aanda.org/10.1051/0004-6361/202039761>
- Breunig, M. M., Kriegel, H.-P., Ng, R. T., & Sander, J. 2000, *ACM SIGMOD Record*, 29, 93. [http://doi.wiley.com/10.1016/S0020-7292\(00\)2809\(0\)2960373-8](http://doi.wiley.com/10.1016/S0020-7292(00)2809(0)2960373-8)<https://dl.acm.org/doi/10.1145/335191.335388>
- Brown, A. G. A., Vallenari, A., Prusti, T., et al. 2018, *Astronomy & Astrophysics*, 616, A1. <https://www.aanda.org/10.1051/0004-6361/201833955><https://www.aanda.org/10.1051/0004-6361/201833051>
- Bruzual, G., & Charlot, S. 2003, *Monthly Notices of the Royal Astronomical Society*, 344, 1000. <https://academic.oup.com/mnras/article-lookup/doi/10.1046/j.1365-8711.2003.06897.x>
- Bundy, K., Bershady, M. A., Law, D. R., et al. 2015, *Astrophysical Journal*, 798, arXiv:1412.1482
- Cenarro, A. J., Peletier, R. F., Sánchez-Blázquez, P., et al. 2007, *Monthly Notices of the Royal Astronomical Society*, 374, 664
- Chen, Y.-p., Trager, S. C., Peletier, R. F., et al. 2014, *Astronomy & Astrophysics*, 565, A117. <http://www.aanda.org/10.1051/0004-6361/201322505>
- Cid Fernandes, R., González Delgado, R. M., García Benito, R., et al. 2014, *Astronomy & Astrophysics*, 561, A130. <http://arxiv.org/abs/1307.0562><http://dx.doi.org/10.1051/0004-6361/201321692><http://www.aanda.org/10.1051/0004-6361/201321692>
- Coelho, P. R. 2014, *Monthly Notices of the Royal Astronomical Society*, 440, 1027
- Coelho, P. R. T., Bruzual, G., & Charlot, S. 2020, *Monthly Notices of the Royal Astronomical Society*, 491, 2025
- Conroy, C. 2013, *Annual Review of Astronomy and Astrophysics*, 51, 393. <http://arxiv.org/abs/1301.7095>
- Conroy, C., Gunn, J. E., & White, M. 2009, *Astrophysical Journal*, 699, 486
- Cui, X.-Q., Zhao, Y.-H., Chu, Y.-Q., et al. 2012, *Research in Astronomy and Astrophysics*, 12, 1197. <http://engine.scichina.com/doi/10.1360/N972015-00975><https://iopscience.iop.org/article/10.1088/1674-4527/12/9/003>
- Dawson, K. S., Kneib, J.-P., Percival, W. J., et al. 2016, *The Astronomical Journal*, 151, 44
- Drory, N., MacDonald, N., Bershady, M. A., et al. 2015, *Astronomical Journal*, 149, 77. <http://dx.doi.org/10.1088/0004-6256/149/2/77>
- Escala, I., Gilbert, K. M., Kirby, E. N., et al. 2020, *The Astrophysical Journal*, 889, 177. <https://iopscience.iop.org/article/10.3847/1538-4357/ab6659>
- Evans, D., Riello, M., De Angeli, F., et al. 2018, 4
- Fernández-Alvar, E., Carigi, L., Allende Prieto, C., et al. 2017, *Monthly Notices of the Royal Astronomical Society*, 465, 1586
- Fix, E., & Hodges, J. 1951, *Randolph Field, Texas, Project.*, 21
- Fluks, M. A., Plez, B., The, P. S., et al. 1994, *A&AS*, 105, 311
- García Pérez, A. E., Prieto, C. A., Holtzman, J. A., et al. 2016, *The Astronomical Journal*, 151, 144. <http://dx.doi.org/10.3847/0004-6256/151/6/144>
- Ginsburg, A., Sipőcz, B. M., Brasseur, C. E., et al. 2019, *AJ*, 157, 98
- Green, G. 2018, *The Journal of Open Source Software*, 3, 695
- Hasselquist, S., Zasowski, G., Feuillet, D. K., et al. 2020, arXiv, arXiv:2008.03603
- Hauschildt, P. H., Allard, F., & Baron, E. 1999, *The Astrophysical Journal*, 512, 377. <https://iopscience.iop.org/article/10.1086/306745>
- Hayden, M. R., Bovy, J., Holtzman, J. A., et al. 2015, *Astrophysical Journal*, 808, arXiv:1503.02110
- Helmi, A., Babusiaux, C., Koppelman, H. H., et al. 2018, *Nature*, 563, 85
- Holtzman, J. A., Hasselquist, S., Shetrone, M., et al. 2018, arXiv, 156, 125. <http://dx.doi.org/10.3847/1538-3881/aad4f9>
- Hunter, J. D. 2007, *Computing in Science & Engineering*, 9, 90
- Husser, T. O., Wende-Von Berg, S., Dreizler, S., et al. 2013, *Astronomy and Astrophysics*, 553, 1
- Ivezić, Ž., Connolly, A. J., VanderPlas, J. T., & Gray, A. 2019, *Statistics, Data Mining, and Machine Learning in Astronomy* (Princeton University Press), doi:10.2307/j.ctvrk1hs. <http://www.jstor.org/stable/10.2307/j.ctvrk1hs>
- Kirby, E. N. 2011, *Publications of the Astronomical Society of the Pacific*, 123, 531
- Kirby, E. N., Gilbert, K. M., Escala, I., et al. 2020, *The Astronomical Journal*, 159, 46
- Knowles, A. T., Sansom, A. E., Allende Prieto, C., & Vazdekis, A. 2021, *Monthly Notices of the Royal Astronomical Society*, 504, 2286

- Kollmeier, J. A., Zasowski, G., Rix, H. W., et al. 2017, arXiv, arXiv:1711.03234
- Lancon, A., & Rocca-Volmerange, B. 1992, *A&AS*, 96, 593
- Law, D. R., Yan, R., Bershad, M. A., et al. 2015, *Astronomical Journal*, 150, 19.
<http://dx.doi.org/10.1088/0004-6256/150/1/19>
- Le Borgne, J. F., Bruzual, G., Pelló, R., et al. 2003, *Astronomy and Astrophysics*, 402, 433
- Lee, Y. S., Beers, T. C., Sivarani, T., et al. 2008, *Astronomical Journal*, 136, 2022
- Lejeune, T., Cuisinier, F., & Buser, R. 1997, *Astronomy and Astrophysics Supplement Series*, 125, 229
- Lejeune, T., Cuisinier, F., & Buser, R. 1998, *A&AS*, 130, 65
- Majewski, S. R., Schiavon, R. P., Frinchaboy, P. M., et al. 2017, *The Astronomical Journal*, 154, 94.
<http://dx.doi.org/10.3847/1538-3881/aa784d>
- Maraston, C. 2005, *Monthly Notices of the Royal Astronomical Society*, 362, 799
- Maraston, C., Greggio, L., Renzini, A., et al. 2003, *Astronomy and Astrophysics*, 400, 823
- Nandakumar, G., Hayden, M. R., Sharma, S., et al. 2020, 21, 1. <http://arxiv.org/abs/2011.02783>
- Ness, M., Hogg, D. W., Rix, H. W., Ho, A. Y., & Zasowski, G. 2015, *Astrophysical Journal*, 808, 16.
<http://dx.doi.org/10.1088/0004-637X/808/1/16>
- Oliphant, T. E. 2006, *A guide to NumPy*, Vol. 1 (Trelgol Publishing USA)
- Pedregosa, F., Varoquaux, G., Gramfort, A., et al. 2011a, *Journal of Machine Learning Research*, 12, 2825
- . 2011b, *Journal of Machine Learning Research*, 12, 2825
- Price-Whelan, A. M., Sipőcz, B., Günther, H., et al. 2018, *The Astronomical Journal*, 156, 123
- Sánchez-Blázquez, P., Peletier, R. F., Jiménez-Vicente, J., et al. 2006, *Monthly Notices of the Royal Astronomical Society*, 371, 703.
<http://arxiv.org/abs/astro-ph/0607009>
<http://dx.doi.org/10.1111/j.1365-2966.2006.10699.x>
<https://academic.oup.com/mnras/article-lookup/doi/10.1111/j.1365-2966.2006.10699.x>
- Sharma, S., Hayden, M. R., Bland-Hawthorn, J., et al. 2020, arXiv, arXiv:2011.13818
- Smee, S. A., Gunn, J. E., Uomoto, A., et al. 2013, *Astronomical Journal*, 146,
[doi:10.1088/0004-6256/146/2/32](https://doi.org/10.1088/0004-6256/146/2/32)
- Terndrup, D. M., Frogel, J. A., & Whitford, A. E. 1990, *ApJ*, 357, 453
- Troyanskaya, O., Cantor, M., Sherlock, G., et al. 2001, *Bioinformatics*, 17, 520
- Valdes, F., Gupta, R., Rose, J. A., Singh, H. P., & Bell, D. J. 2004, *The Astrophysical Journal Supplement Series*, 152, 251
- Van Rossum, G., & Drake, F. L. 2009, *Python 3 Reference Manual* (Scotts Valley, CA: CreateSpace)
- Van Rossum, G., & Drake Jr, F. L. 1995, *Python tutorial* (Centrum voor Wiskunde en Informatica Amsterdam, The Netherlands)
- Vanderplas, J., Connolly, A., Ivezić, Ž., & Gray, A. 2012, in *Conference on Intelligent Data Understanding (CIDU)*, 47–54
- Virtanen, P., Gommers, R., Oliphant, T. E., et al. 2020, *Nature Methods*, 17, 261
- Wake, D. A., Bundy, K., Diamond-Stanic, A. M., et al. 2017, *The Astronomical Journal*, 154, 86.
<http://dx.doi.org/10.3847/1538-3881/aa7ecc>
- Walcher, C. J., Yates, R. M., Minchev, I., et al. 2016, *Astronomy and Astrophysics*, 594, 1
- Waskom, M., Botvinnik, O., O’Kane, D., et al. 2017, *mwaskom/seaborn: v0.8.1* (September 2017), vv0.8.1, Zenodo, [doi:10.5281/zenodo.883859](https://doi.org/10.5281/zenodo.883859).
<https://doi.org/10.5281/zenodo.883859>
- Xiang, M. S., Liu, X. W., Yuan, H. B., et al. 2015, *Monthly Notices of the Royal Astronomical Society*, 448, 822
- Yan, R., Bundy, K., Law, D. R., et al. 2016, *The Astronomical Journal*, 152, 197
- Yan, R., Chen, Y., Lazarz, D., et al. 2019, *The Astrophysical Journal*, 883, 175. <https://iopscience.iop.org/article/10.3847/1538-4357/ab3ebc>
- Yanny, B., Rockosi, C., Newberg, H. J., et al. 2009, *Astronomical Journal*, 137, 4377